AD-A042 330   OHIO STATE UNIV   COLUMBUS ELECTROSCIENCE LAB   F/G 9/5
PATTERN PREDICTION OF ANTENNAS ON A FLAT PLATE.(U)
MAR 77   G K CHAN, G A THIELE   N00014-75-C-0313
UNCLASSIFIED   ESL-4091-4   NL

| OF |
AD
A042330

END
DATE
FILMED
8-77
DDC

73
NW

528,083

③

FINAL REPORT

PATTERN PREDICTION OF ANTENNAS ON A FLAT PLATE

G. K. Chan and G. A. Thiele

The Ohio State University

ElectroScience Laboratory

Department of Electrical Engineering
Columbus, Ohio 43212

FINAL REPORT 4091-4

March 1977

Contract N00014-75-C-0313

D D C

AUG 3 1977

C

SECURITY CLASSIFICATION OF THIS PAGE *(When Data Entered)*

REPORT DOCUMENTATION PAGE		READ INSTRUCTIONS BEFORE COMPLETING FORM
1. REPORT NUMBER	2. GOVT ACCESSION NO.	3. RECIPIENT'S CATALOG NUMBER 528083
4. TITLE *(and Subtitle)* FINAL REPORT — PATTERN PREDICTION OF ANTENNAS ON A FLAT PLATE.		5. TYPE OF REPORT & PERIOD COVERED Final Report.
		6. PERFORMING ORG. REPORT NUMBER ESL-4091-4
7. AUTHOR(s) G. K. Chan and G. A. Thiele		8. CONTRACT OR GRANT NUMBER(s) Contract N00014-75-C-0313
9. PERFORMING ORGANIZATION NAME AND ADDRESS The Ohio State University ElectroScience Laboratory, Department of Electrical Engineering Columbus, Ohio 43212		10. PROGRAM ELEMENT PROJECT, TASK AREA & WORK UNIT NUMBERS NRL Req. N00173-75-RQ-06141
11. CONTROLLING OFFICE NAME AND ADDRESS Department of the Navy Office of Naval Research Arlington, Virginia 22217		12. REPORT DATE March 1977
		13. NUMBER OF PAGES 53
14. MONITORING AGENCY NAME & ADDRESS(if different from Controlling Office)		15. SECURITY CLASS. *(of this report)* Unclassified
		15a. DECLASSIFICATION DOWNGRADING SCHEDULE

16. DISTRIBUTION STATEMENT *(of this Report)*

Reproduction in whole or in part is permitted for any purpose
of the United States Government.

APPROVED FOR PUBLIC RELEASE
DISTRIBUTION UNLIMITED

17. DISTRIBUTION STATEMENT *(of the abstract entered in Block 20, if different from Report)*

18. SUPPLEMENTARY NOTES

19. KEY WORDS *(Continue on reverse side if necessary and identify by block number)*

Antennas
Satellite
Moment Methods
Geometrical Theory of Diffraction

20. ABSTRACT *(Continue on reverse side if necessary and identify by block number)*

A technique which combines the Method of Moments and the Geometrical Theory of Diffraction into a single Hybrid Technique is described and applied to the problem of computing the performance of wire type antennas on a planar satellite panel. Where possible results are compared with independently derived calculations or measurements to verify the computer program. The computer program, which is not included in the report, is capable of handling up to five antennas on a single satellite metallic panel.

DD FORM 1473 1 JAN 73   EDITION OF 1 NOV 65 IS OBSOLETE

402251

ACKNOWLEDGMENT

The first named author (G.K. Chan) would like to express his sincere gratitude to Dr. W.D. Burnside, Dr. R.J. Marhefka and Dr. N. Wang for their help and ideas.

TABLE OF CONTENTS

I. INTRODUCTION

Previous work done in connection with the present research program has utilized two modern computational methods in electromagnetics. The first technique is the Geometrical Theory of Diffraction or GTD, which is most often used when an antenna radiates from a structure that is large in terms of the wavelength. The second technique is the Method of Moments which, for practical reasons based on computer storage, applies best to structures that are not large in terms of the wavelength.

A major innovation of the research performed in connection with the prediction of satellite antenna radiation patterns lies in the formal combination of the GTD and the moment method into a single computational method known as the Hybrid Technique [1]. This technique was used by Moore and Thiele [2] to investigate a turnstyle type antenna on a 24" x 24" satellite panel.

The computer program developed in connection with the turnstyle antenna investigation was limited to monopole type elements and pattern calculations in one plane only. Subsequent work described in this report has been concerned with the generalization of the theory and the incorporation of that theory into the computer program so that it may be used in the analysis and design of more general satellite antenna systems than previously possible.

II. THE HYBRID TECHNIQUE

The Hybrid Technique is actually an extension of the moment method accomplished by modifying the impedance matrix to include the GTD.

A. Moment Method

Consider a general perfectly conducting body on which there is a current density $\bar{J}$. In order to satisfy the boundary condition everywhere on the body surface, the total tangential electric field has to be zero. That is,

$$E^S_{tan} + E^i_{tan} = 0 \qquad (2-1)$$

where E^i_{tan} is the tangential component of the incident electric field due to a source located anywhere outside the body and E^S_{tan} is the tangential component of the scattered electric field radiated by the current $\bar{J}$ on the conducting body. For simplicity, the subscript "tan" is dropped and it is understood that only the tangential electric field is being applied to satisfy the boundary condition on the body surface.

To apply the moment method to find the unknown response $\bar{J}$ with $\bar{E}^i$ as the known excitation, write the functional operator equation [3,4] to relate the $\bar{J}$ and $\bar{E}^i$ as

1

$$L_{op}(\bar{J}) = \bar{E}^i \tag{2-2}$$

where L_{op} represents the integral functional operator. For a unique solution, L_{op} must have a corresponding inverse operator, L_{op}^{-1}, such that

$$L_{op}^{-1} (\bar{E}^i) = \bar{J} \quad . \tag{2-3}$$

In addition, an inner product, obtained by integrating $\bar{J} \cdot \bar{E}$ over the surface under consideration to obtain the reaction $\bar{J}, \bar{E}$ [5], is defined to satisfy the following symmetric inner product axioms:

$$\langle \alpha \bar{J}_1 + \beta \bar{J}_2, \bar{E} \rangle = \langle \alpha \bar{J}_1, \bar{E} \rangle + \langle \beta \bar{J}_2, \bar{E} \rangle \tag{2-4}$$

$$\langle \bar{J}, \bar{E} \rangle = \langle \bar{E}, \bar{J} \rangle \tag{2-5}$$

$$\langle \bar{J}^\star, \bar{J} \rangle = 0 \quad \text{if and only if } \bar{J} = 0$$
$$> 0 \quad \text{if } \bar{J} \neq 0 \tag{2-6}$$

where α and β are scalars and $\star$ denotes complex conjugation.

Next we expand the current $\bar{J}$ on the surface of the conducting body in a series of basis functions $\{\bar{J}_1, \bar{J}_2, \cdots \bar{J}_n\}$ defined in the domain of L_{op}. That is,

$$\bar{J} = \sum_{n=1}^{N} I_n \bar{J}_n \tag{2-7}$$

where I_n are the complex coefficients to be determined.

Substituting Equation (2-7) into Equation (2-2), using the linearity of the operator, and forming the inner product with a set of weight functions $\{\bar{W}_1, \bar{W}_2 \cdots, \bar{W}_m\}$ in the domain of L_{op}, we then obtain

$$\sum_{n=1}^{N} I_n \langle \bar{W}_m, L_{op}(\bar{J}_n) \rangle = \langle \bar{W}_m, \bar{E}^i \rangle \tag{2-8}$$

2

Actually, Equation (2-8) represents the mth row of equations in a system of N such equations while the quantity $L_{op}(\bar{J}_n)$ represents the electric field from the nth basis function of unit amplitude. In the usual moment method matrix notation, Equation (2-8) can be written as

$$[Z] [I] = [V] \tag{2-9}$$

where $[Z]$, $[I]$ and $[V]$ are called the generalized impedance matrix, the generalized current matrix and generalized voltage matrix, respectively. The elements of $[Z]$ are denoted by

$$Z_{mn} = \langle \bar{W}_m, L_{op}(\bar{J}_n) \rangle \quad . \tag{2-10}$$

To include the diffracted field contribution from the nth basis function $\bar{J}_n$, a new matrix element can be written as

$$Z'_{mn} = \langle \bar{W}_m, L_{op}(\bar{J}_n) + c\, L_{op}(\bar{J}_n) \rangle \tag{2-11}$$

or, by axioms (2-4) and (2-5),

$$Z'_{mn} = \langle \bar{W}_m, L_{op}(\bar{J}_n) \rangle + \langle \bar{W}_m, c\, L_{op}(\bar{J}_n) \rangle \tag{2-12}$$

where $c\, L_{op}(\bar{J}_n)$ represents the contribution from GTD and c is a complex quantity. Equation (2-12) may be further simplified as

$$Z'_{mn} = Z_{mn} + Z^g_{mn} \tag{2-13}$$

where $Z^g_{mn} = \langle \bar{W}_m, c\, L_{op}(\bar{J}_n) \rangle$. With the new matrix element, Equation (2-9) can be rewritten as

$$[Z'] [I'] = [V] \tag{2-14}$$

where $[I']$ is the current distribution on the conducting body surface, including the contribution from GTD.

3

B. Diffraction Theory

The problem of straight edge diffraction by a perfectly-conducting wedge was first solved by Sommerfeld [6]. Later, Pauli [7] introduced the V_β function as a practical formulation in the solution for the fields diffracted by a perfectly-conducting wedge of finite angle. More recently, Hutchins and Kouyoumjian presented a formulation which yields better accuracy than Pauli's solution in the transition regions near the incident and reflected shadow boundaries, particularly when $r < \lambda$. Their formulation can be written as

$$V_B(L,\beta,n) = I_{-\pi}(L,\beta,n) + I_{+\pi}(L,\beta,n) \qquad (2\text{-}15)$$

where

$$I_{\pm\pi}(L,\beta,n) \sim \frac{e^{-j(kL+\pi/4)}}{jn\sqrt{2\pi}} \sqrt{a} \cot\left(\frac{\pi \pm \beta}{2n}\right) e^{jkLa}$$

$$\cdot \int_{\sqrt{kLa}}^{\infty} e^{-jt^2} dt + [\text{higher order terms}] \qquad (2\text{-}16)$$

and

$$a = 1 + \cos(\beta - 2n\pi N) \qquad (2\text{-}17)$$

The higher order terms are negligible for large kL and n is defined from the wedge angle $WA = (2-n)\pi$ as shown in Figure 2-1. Moreover, N is a positive or negative integer or zero whichever most nearly satisfies the equation

$$2n\pi N - \beta = -\pi \quad \text{for } I_{-\pi} \qquad (2\text{-}18)$$

and

$$2n\pi N - \beta = \pi \quad \text{for } I_{+\pi} \qquad . \qquad (2\text{-}19)$$

The distance parameter L and β are defined subsequently.

4

OBSERVATION POINT

$\hat{I} = \hat{\beta}_0' \times \hat{\phi}'$

$\hat{s} = \hat{\beta}_0 \times \hat{\phi}$

$(2-n)\pi$

CONE OF
DIFFRACTED RAYS

Q_E

β_0

$\hat{s}$

$\hat{\beta}_0$

β_0

$\hat{\beta}_0'$

$\hat{I}$

S'

SOURCE POINT
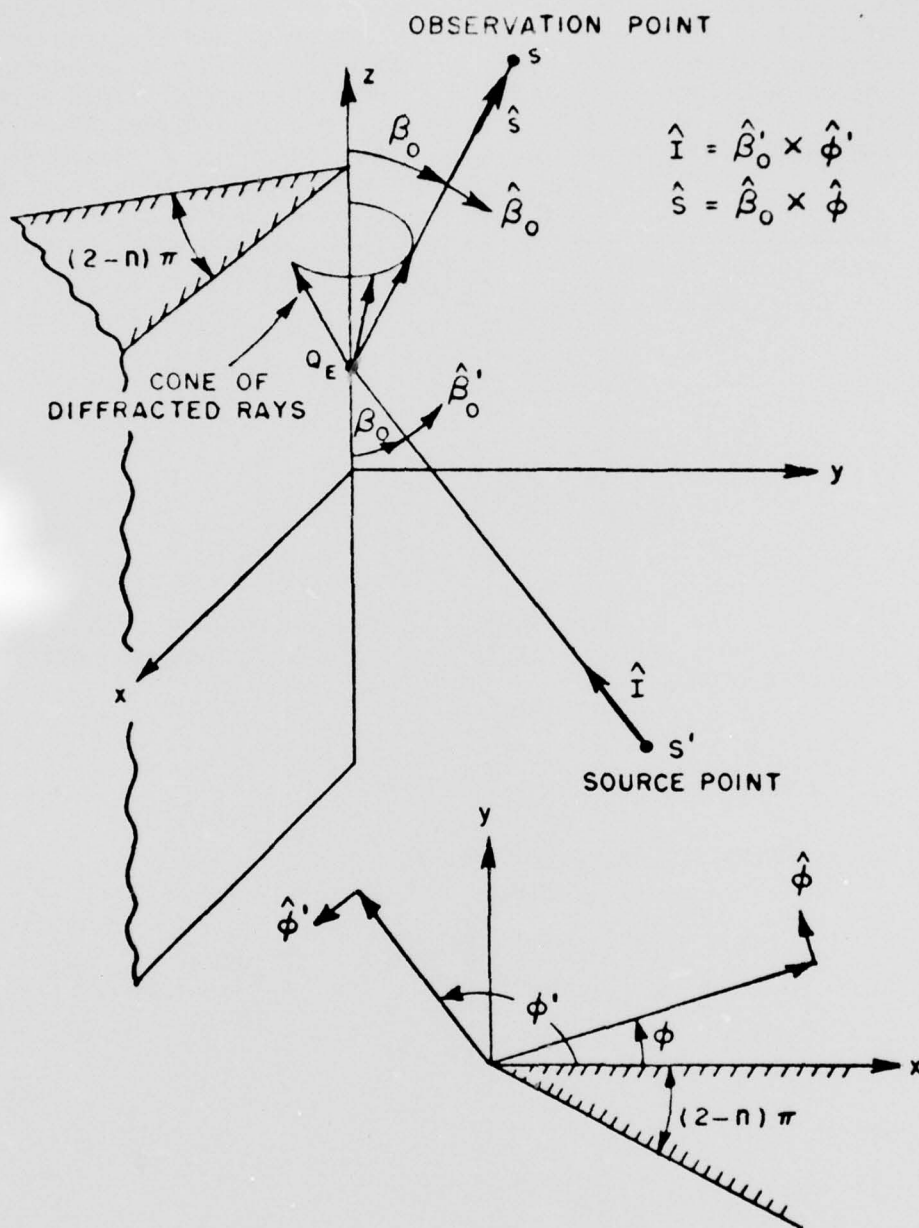
$\hat{\phi}'$

$\hat{\phi}$

ϕ'

ϕ

$(2-n)\pi$

Figure 2-1.   Geometry for 3-dimensional diffraction
problem.

5

Consider Figure 2-1 with source field $\bar{E}^i(s)$ from a source located at point $s'(\rho',\phi',z')$. The source can be either electric or magnetic giving rise to either plane, cylindrical, conical or spherical wave incidence on the wedge tip. The diffracted vector field at the point $s(\rho,\phi,z)$ can be written in terms of a dyadic diffraction coefficient. Kouyoumjian and Pathak [3] have shown that the diffracted field can be written compactly if they are expressed in terms of a ray fixed coordinate system centered at the point or points of diffraction Q_E. The relationships between the orthogonal unit vectors associated with these coordinates $(\hat{s}',\hat{\beta}_0',\hat{\phi}';\hat{s},\hat{\beta}_0,\hat{\phi})$ are given by

$$\hat{I} = -\hat{s}' \tag{2-20}$$

$$\hat{I} = \hat{\beta}_0' \times \hat{\phi}' \tag{2-21}$$

$$\hat{s} = \hat{\beta}_0 \times \hat{\phi} \tag{2-22}$$

where $\hat{I}$ is the incident direction unit vector, and $\hat{s}$ is the diffraction direction unit vector. In this coordinate system, the diffracted field may be written as

$$\bar{E}^d(s) \sim \bar{E}^i(Q_E) \cdot \bar{\bar{D}}(\hat{s},\hat{I}) A(s) e^{-jks} \tag{2-23}$$

or, in terms of the V_B function as

$$\begin{bmatrix} E_{\parallel}^d(s) \\ E_{\perp}^d(s) \end{bmatrix} \sim \begin{bmatrix} -V_B^- & 0 \\ 0 & -V_B^+ \end{bmatrix} \begin{bmatrix} E_{\parallel}^i(Q_E) \\ E_{\perp}^i(Q_E) \end{bmatrix} \frac{\sqrt{L} \, e^{jkL}}{\sin\beta_0} A(s) \, e^{-jks} \tag{2-24}$$

where

$$E_{\parallel}^d(s) = \bar{E}^d(s) \cdot \hat{\beta} \tag{2-25}$$

$$E_{\perp}^d(s) = \bar{E}^d(s) \cdot \hat{\phi} \tag{2-26}$$

and

$$V_B^{\mp} = V_B(L,\beta^-,n) \mp V_B(L,\beta^+,n) \quad . \tag{2-27}$$

6

The minus sign of the V_B function is used for the soft case (E field parallel to the edge) and the positive sign is for the hard case (E field perpendicular to the edge). The angular relations are given by $\beta = \beta^{\mp} = \phi \mp \phi'$ where the β^{-} term is associated with the incident field and the β^{+} term with the reflected field. The ray divergence factor or spatial attenuation factor $A(s)$ is given by

$$A(s) = \begin{cases} \dfrac{1}{\sqrt{s}} & \text{for plane, cylindrical and} \\ & \text{conical wave incidence} \\[2em] \sqrt{\dfrac{s'}{s(s+s')}} & \text{for spherical wave} \\ & \text{incidence} \end{cases} \qquad (2\text{-}28)$$

and L is given by

$$L = \begin{cases} s \sin^2 \beta_0 & \text{for plane wave} \\ & \text{incidence} \\[1em] \dfrac{\rho'\rho}{\rho'+\rho} & \text{for cylindrical wave} \\ & \text{incidence} \\[1em] \dfrac{s's \sin^2\beta_0}{s+s'} & \text{for conical and spherical} \\ & \text{wave incidence} \end{cases} \qquad 2\text{-}29)$$

It is the introduction of the distance parameter L by Pathak and Kouyoumjian that permits near-zone to near-zone diffraction to be obtained accurately for $kL>1$.

III. APPLICATION OF THE HYBRID TECHNIQUE

Examples

A. Monopole near a Conducting Wedge

Consider the conical problem of a monopole near a perfectly-conducting wedge as shown in Figure 3-1a. Assume that the monopole is a thin wire with radius, $R<<\lambda$ and its axis coincides with the coordinate z-axis. To find the current distribution on the monopole, first apply the boundary condition on the wire surface. That is,

$$- E_z^s(0,z) = E_z^i(0,z) \qquad (3\text{-}1)$$

or

$$L_{op}(\overline{J}) = - \overline{E}^s(0,z) = \overline{E}_z^i(0,z) \qquad (3\text{-}2)$$

where $\overline{E}^s(0,z)$ may be expressed as [9]

7

$\hat{z}$

2R

m

d

H

n

$\hat{x}$

y

WA = (2−n)π

(a)

$\hat{z}$

DIFFRACTED FIELD

DIRECT FIELD

$\hat{\phi}$

$\hat{\phi}$

s

m

s'

ϕ

n

ϕ'

Q_E

$\hat{y}$

WA = (2−n)π

(b)

Figure 3-1. (a) Monopole near a perfectly conducting wedge.
(b) The direct and diffracted fields caused
by the nth source segment incident upon
the mth observation segment.

8

$$E_z^s(0,z) = \frac{1}{4\pi j\omega\varepsilon} \int_{-H}^{H} J(z') \frac{e^{-jkr}}{r^5} [(1+jkr)(2r^2-3R^2)+(kRr)^2)]dz'$$

$$(3-3)$$

where z' and z denote the source point and observation point, respectively, and

$$r = [R^2 + (z-z')^2]^{1/2}$$

$$(3-4)$$

Therefore, L_{op} can be defined as

$$L_{op} = \frac{-\lambda \sqrt{\frac{\mu}{\varepsilon}}}{8\pi^2 j} \int_{-H}^{H} G(r,r') \, dz'$$

$$(3-5)$$

where

$$G(r,r') = \frac{e^{-jkr}}{r^5} [(1+jkr)(2r^2-3R^2)+(kRr)^2]$$

$$(3-6)$$

Then the current distribution $\bar{J}(z')$ may be expanded by a finite set of piecewise sinusoidal basis functions [10], $\{\bar{F}_1(z'),\bar{F}_2(z')\cdots\bar{F}_N(z')\}$ as shown in Figure 3-2. That is,

$$\bar{J}(z') = \sum_{n=1}^{N} I_n \bar{F}_n(z')$$

$$(3-7)$$

Where I_n is a complex quantity and

$$\bar{F}_n(z') = \frac{\sinh k\,(z'-z_{n-1})}{\sinh k\,(z_n-z_{n-1})} \, \hat{z} + \frac{\sinh k\,(z_{n+1}-z')}{\sinh k\,(z_{n+1}-z_n)} \, \hat{z}$$

$$(3-8)$$

k is the complex propagation constant of homogeneous medium:

$$k = j\omega\sqrt{\mu\varepsilon}$$

$$(3-9)$$

Thus, Equation (3-2) can be written as

$$\sum_{n=1}^{N} I_n L_{op} (\bar{F}_n(z')) = - \bar{E}^s(0,z)$$

$$(3-10)$$

9
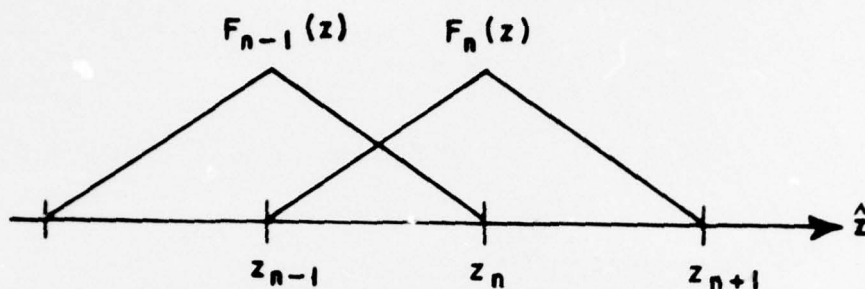
Figure 3-2. Piecewise sinusoidal basis functions.

Next, with a set of weighing functions defined as

$$\overline{W}_m = \overline{F}_m(z') \tag{3-11}$$

the matrix element Z_{mn} in Equation (2-13) can be calculated by

$$Z_{mn} = <\overline{F}_m(z'), L_{op} (\overline{F}_n(z')> \tag{3-12}$$

which is physically interpreted as the direct field contribution at region m due to a unit of piecewise sinusoidal current $\overline{F}_n(z')$ defined at region n as shown in Figure 3-1b. Also, the matrix element ΔZ_{mn}^g in Equation (2-13) that accounts for the diffracted field from the edge of the wedge due to the same basis function $\overline{F}_n(z')$ can be written as

$$\Delta Z_{mn}^g = <\overline{F}_m(z'), \overline{E}_n^d(s)> = \int \overline{F}_m(s) \cdot \overline{E}_n^d(s) \, dz \tag{3-13}$$

where $\overline{E}_n^d(s)$, the diffracted field arriving at region m, is obtained using GTD and the integral is over the length of region m. That is,

$$\overline{E}_n^d(s) \sim -V_B^+ E_\perp^i(Q_E) \frac{\sqrt{L}}{\sin\beta_o} e^{jkL} A(s) e^{-jks} \hat{\phi} \tag{3-14}$$

where $E_\perp^i(Q_E)$ is the incident field component perpendicular to the edge due to the current basis function $\overline{F}_n(z')$ and ϕ is defined as shown in

10

Figure 3-1b. In this particular case, $E_{||}^i(Q_E)$, the incident field component parallel to the edge equals zero, and the incident angle is $\beta_0 = \pi/2$. Moreover, for sperical wave incident $A(s)$ and L are defined by Equation (2-28) and Equation (2-29), respectively. Therefore, Equation (3-14) can further be simplified as .

$$\overline{E}_n^d(s) \sim -V_B^+ \, E_\perp^i(Q_E) \, \frac{s'}{s+s'} \, e^{jk\left[\frac{s's}{s'+s} - s\right]} \, \hat{\phi} \quad . \tag{3-15}$$

With $Z_{mn}' = z_{mn} + Z_{mn}^g$ calculated, the unknown current distribution on the monopole can then be obtained by solving the matrix equation

$$[I'] = [Z']^{-1} [V] \quad . \tag{3-16}$$

B. Monopoles on a Rectangular Ground Plane

In general, given the locations of a source, an observation point and the edge of a wedge, it is necessary to determine if the given edge has a diffraction point that will give a diffraction contribution in the observation direction. The equations derived below can be referred to [11,12].

From Figure 3-3, the position vector $\overline{RD}$ of a diffraction point Q_E can be obtained as follows:

$$\overline{RQ} = \overline{C2} - |[(\overline{RS} - \overline{C2}) \cdot \hat{E}]| \hat{E} \tag{3-17}$$

$$W = (\overline{RO} - \overline{RQ}) \cdot \hat{E} \tag{3-18}$$

$$\overline{RP} = \overline{RQ} + W\hat{E} \tag{3-19}$$

$$G = |\overline{RO} - \overline{RP}| \tag{3-20}$$

$$H = |\overline{RS} - \overline{RQ}| \tag{3-21}$$

$$\overline{RD} = \overline{RP} - \left(\frac{WG}{G+H}\right) \hat{E} \tag{3-22}$$

Diffraction occurs only if the following inequality is satisfied.

$$\frac{(\overline{C1} - \overline{RS})}{|\overline{C1} - \overline{RS}|} \cdot \hat{E} < \hat{D} \cdot \hat{E} < \frac{(\overline{C2} - \overline{RS})}{|\overline{C2} - \overline{RS}|} \cdot \hat{E} \quad . \tag{3-23}$$

11
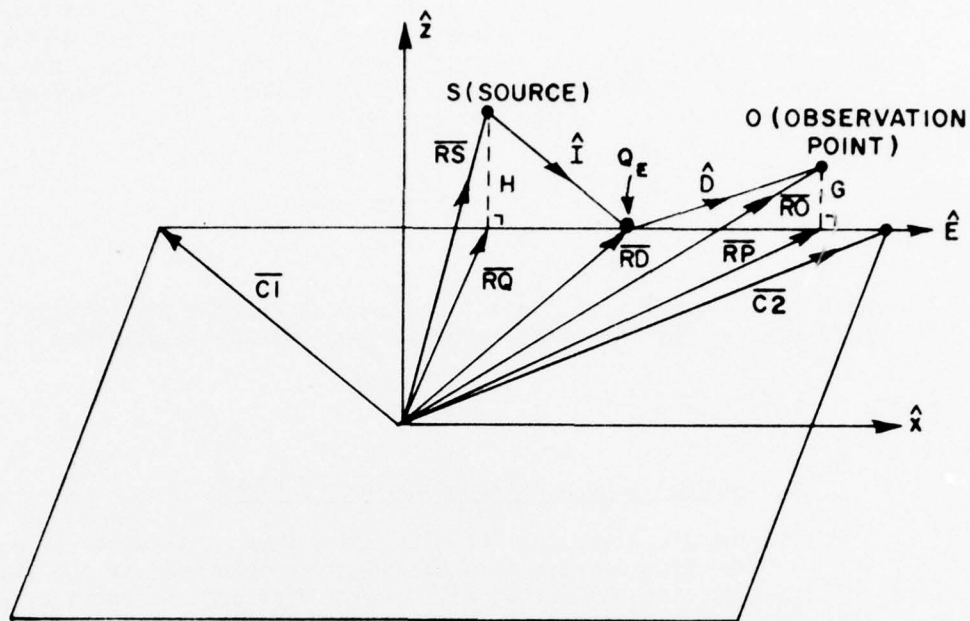
Figure 3-3. Geometry for the calculation of the position
vector $\overline{RD}$ of a diffraction point Q_E.

After $\overline{RD}$ is calculated, the same procedure as in Example A will give the
current distributions on monopoles on the ground plane in the presence
of the diffracting edges. To determine the far field pattern including
the four edges of diffraction, it is necessary to define the incident and
reflection shadow boundaries as shown in Figure 3-4.

From Figure 3-5a, it is obvious that only if the sign of

$$\hat{n} \cdot (\overline{RS} - \overline{CT}) \text{ and } \hat{n} \cdot \hat{D} \tag{3-24}$$

are the same and the intersection point is not on the rectangular plate,
then the observation point is in the direct incidence region. If $\overline{RS}$
represents the location of the image of a source and if the intersection
point is on the rectangular plate, then the opposite sign of Equation (3-24)
indicates that the observation point is within the reflection region as
shown in Figure 3-5b. The location of intersection point is defined as
follows (see Figure 3-5c).

$$M = - \frac{(\overline{RS} - \overline{CT}) \cdot \hat{n}}{\hat{D} \cdot \hat{n}} \tag{3-25}$$

12
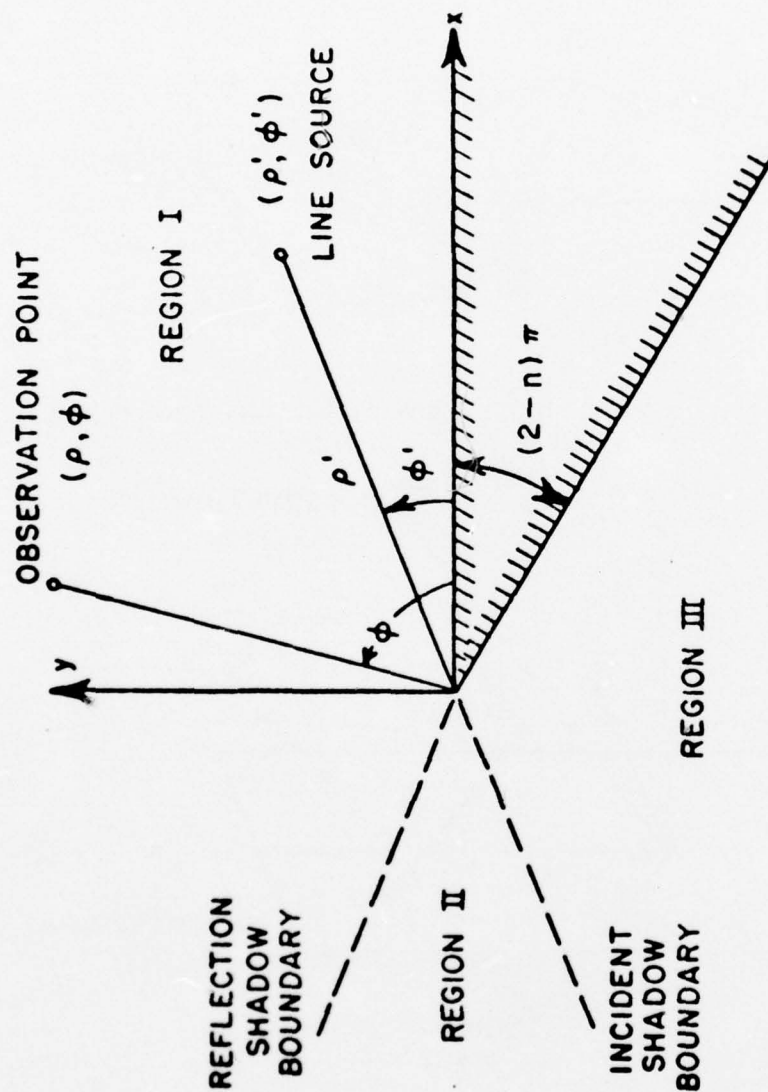
Figure 3-4. Geometry of a 2-dimensional diffraction problem. Region I consists of direct field, reflected field and diffracted field. Region II consists of direct field and diffracted field. Region III (shadow region) consists of diffracted field only.

(a)
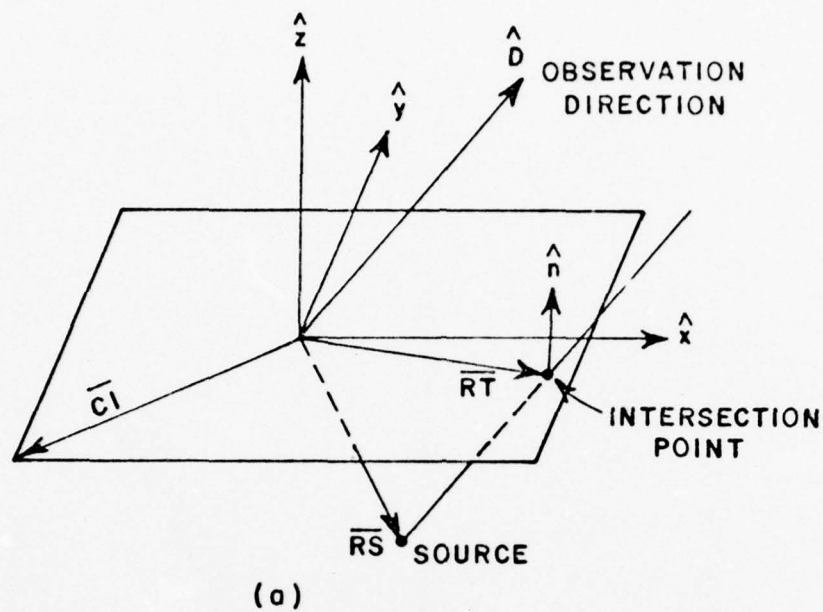
Figure 3-5(a).   Geometry for finding direct incidence region.

(b)
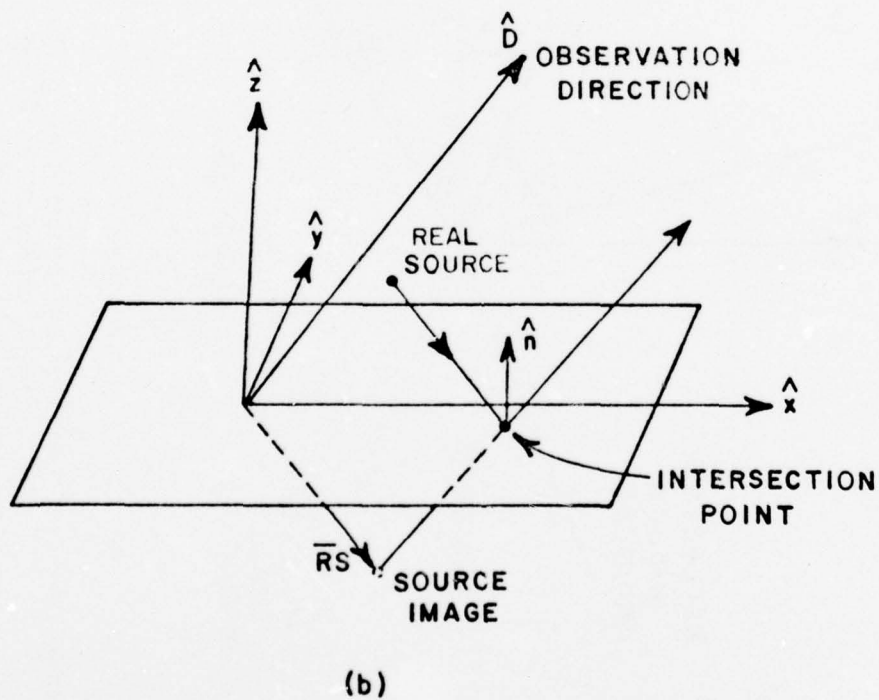
Figure 3-5(b).   Geometry for finding reflection region.

14
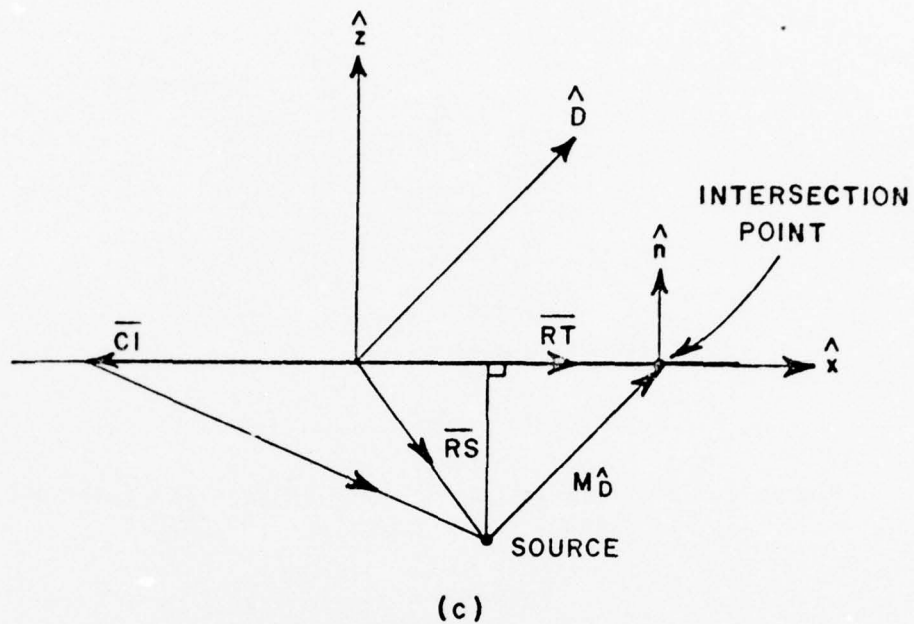
Figure 3-5(c). Geometry for finding the location of intersection point.

$$\overline{RT} = \overline{RS} + M\,\hat{D} \quad . \tag{3-26}$$

To determine if $\overline{RT}$, the interception point, is on the ground plane, the following equation can be tested.

$$\left| \sum_{n=1}^{4} \theta_n \right| \quad \begin{array}{l} < \pi \text{ not on the plate} \\ \\ > \pi \text{ on the plate} \end{array} \tag{3-27}$$

where

$$\theta_n = \tan^{-1} \left\{ \frac{[(\overline{C_n} - \overline{RT}) \times (\overline{C}_{n+1} - \overline{RT})] \cdot \hat{n}}{(\overline{C_n} - \overline{RT}) \cdot (\overline{C}_{n+1} - \overline{RT})} \right\} \tag{3-28}$$

and is defined as shown in Figure 3-6.

15

(a)
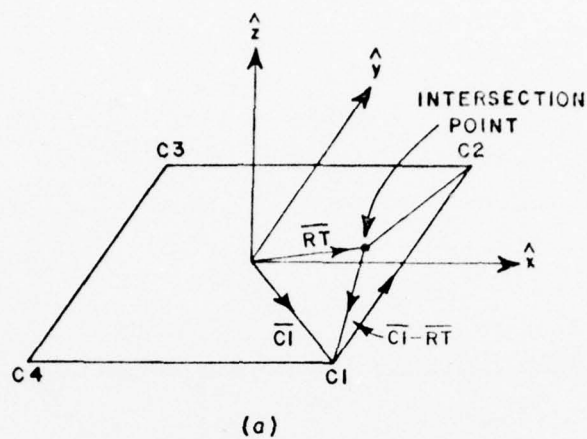
Figure 3-6(b).   The vector relation between the intersection
point and one ground plane corner.

(b)
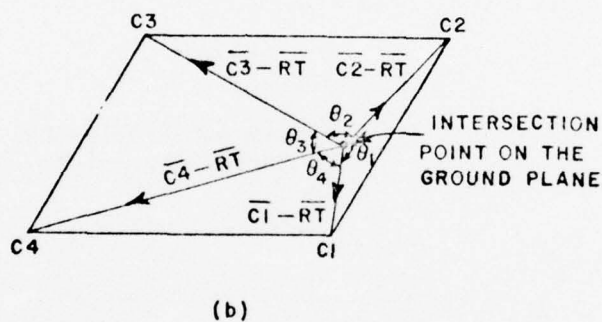
Figure 3-6(b).   When the intersection point is on the ground plane,
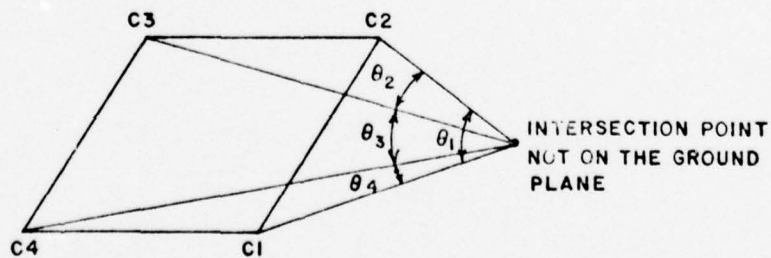
$$\left| \sum_{n=1}^{4} \theta_n \right| > \pi \ .$$

Figure 3-6(c).   When the intersection point is not on the ground plane,

$$\left| \sum_{n=1}^{4} \theta_n \right| < \pi \ .$$

16

To include the diffraction by the four edges to the total far field pattern, requires another set of equations to determine the diffraction points on the four edges, since in far field case, only the observation direction is given and it is assumed that $r \to \infty$.
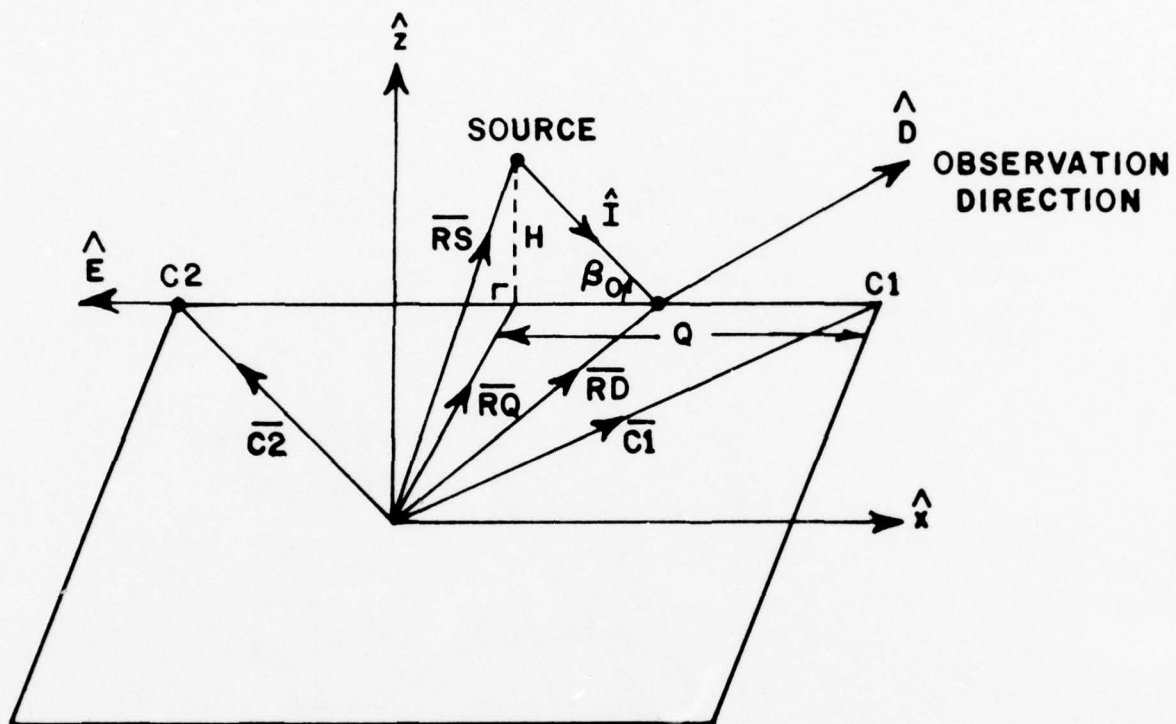
Figure 3-7. Geometry for finding the position vector $\overline{RD}$ of a diffraction point when the far field observation direction $\hat{D}$ is given.

From Figure 3-7, it is easy to show that

$$Q = (\overline{RS} - \overline{CT}) \cdot \hat{E} \tag{3-29}$$

$$H = |(\overline{RS} - \overline{CT}) - Q \, \hat{E}| \tag{3-30}$$

$$\cot \beta_0 = \frac{\hat{D} \cdot \hat{E}}{\sqrt{1 - (\hat{D} \cdot \hat{E})^2}} \tag{3-31}$$

$$\overline{RQ} = \overline{CT} + Q \, \hat{E} \tag{3-32}$$

$$\overline{RD} = \overline{RQ} + (H \cot \beta_0) \, \hat{E} \tag{3-33}$$

where $\overline{RD}$ is the location of diffraction point which must satisfy the following inequality to ensure that diffraction occurs:

$$\frac{(\overline{C1} - \overline{RS})}{|\overline{C1} - \overline{RS}|} \cdot \hat{E} < \hat{D} \cdot \hat{E} < \frac{(\overline{C2} - \overline{RS})}{|\overline{C2} - \overline{RS}|} \cdot \hat{E} \qquad . \tag{3-34}$$

That is, the diffraction points must be defined on the edges.

The total far field pattern is calculated by summing the direct, reflected and diffracted field. The direct and reflected field may be obtained via the moment method while the diffracted field may be determined by the GTD. As mentioned in Section II, the diffracted field can be expressed compactly in terms of a fixed ray coordinate system centered at the point Q_E. The three orthogonal unit vectors of the coordinate system as shown in Figure 3-8 are $\hat{E}$ the unit vector along the
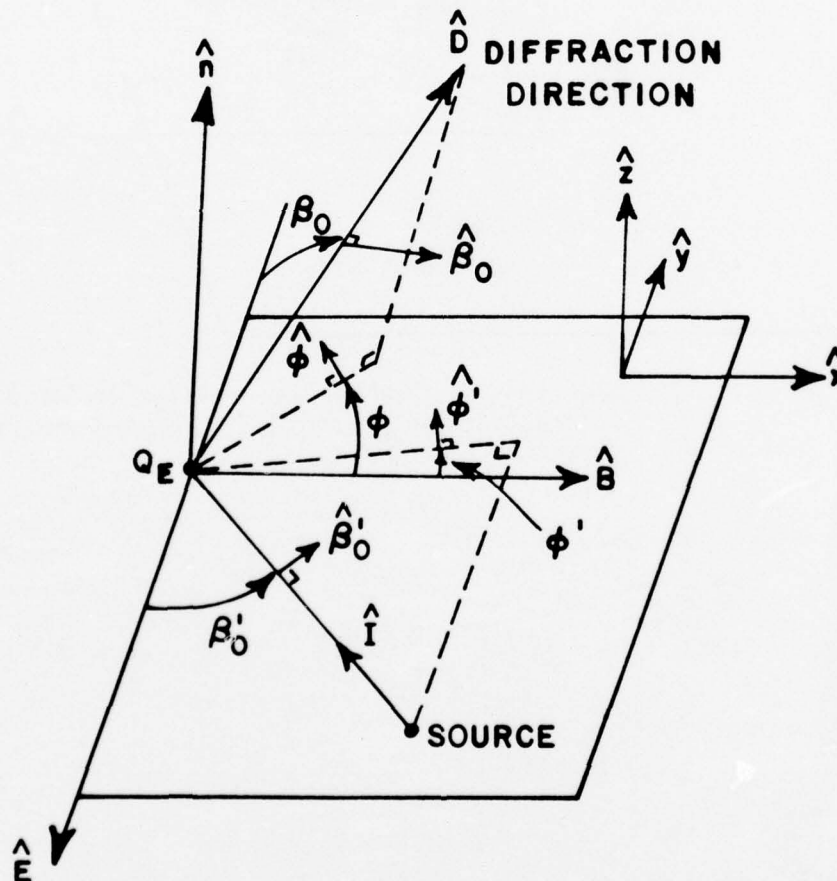
Figure 3-8. Fixed ray coordinate system centered at the diffraction point Q_E.

18

edge, $\hat{n}$ the normal to the surface, and $\hat{B} = \hat{n} \times \hat{E}$. The incident unit vector $\hat{I}$, the diffraction unit vector $\hat{D}$, β_0, β_0', ϕ and ϕ' can then be represented as follows:

$$- \hat{I} = \cos \beta_0' \; \hat{E} + \sin \beta_0' \cos \phi' \; \hat{B} + \sin \beta_0' \sin \phi' \; \hat{n} \tag{3-35}$$

$$\hat{D} = \cos \beta_0 \; \hat{E} + \sin \beta_0 \cos\phi \; \hat{B} + \sin \beta_0 \sin\phi \; \hat{n} \tag{3-36}$$

$$\phi' = \tan^{-1} \left(\frac{-\hat{I} \cdot \hat{n}}{-\hat{I} \cdot \hat{B}} \right) \tag{3-37}$$

$$\phi = \tan^{-1} \left(\frac{\hat{D} \cdot \hat{n}}{\hat{D} \cdot \hat{B}} \right) \tag{3-38}$$

$$\hat{\phi}' = \cos\phi' \; \hat{n} - \sin\phi' \; \hat{B} \tag{3-39}$$

$$\hat{\phi} = \cos\phi \; \hat{n} - \sin\phi \; \hat{B} \tag{3-40}$$

$$\hat{\beta}_0' = \hat{\phi}' \times \hat{I} \tag{3-41}$$

$$\hat{\beta}_0 = \hat{\phi} \times \hat{D} \quad . \tag{3-42}$$

Thereupon, the diffracted field can be expressed as

$$\overline{E}^d = E_{\perp}^d \; \hat{\phi} + E_{\parallel}^d \; \hat{\beta}_0 \tag{3-43}$$

where

$$\begin{bmatrix} E_{\parallel}^d(s) \\ E_{\perp}^d(s) \end{bmatrix} \sim \begin{bmatrix} -V_B^- & 0 \\ 0 & -V_B^+ \end{bmatrix} \begin{bmatrix} E_{\parallel}^i(Q_E) \\ E_{\perp}^i(Q_E) \end{bmatrix} \frac{\sqrt{L}}{\sin\beta_0} \; A(s) \; e^{-jks} \tag{3-44}$$

and

$$E_{\parallel}^i(Q_E) = \overline{E}^i(Q_E) \cdot \hat{\beta}_0' \tag{3-45}$$

$$E_{\perp}^i(Q_E) = \overline{E}^i(Q_E) \cdot \hat{\phi}' \tag{3-46}$$

19

where $\overline{E}^i(Q_E)$ is the incident field at diffraction point Q_E due to the current distribution on the monopoles. For spherical wave incident and for far field calculation ($s\to\infty$), Equation (3-44) can be written as

$$\begin{bmatrix} E^d_\parallel(s) \\ E^d_\perp(s) \end{bmatrix} \sim \begin{bmatrix} -V^-_B & 0 \\ 0 & -V^+_B \end{bmatrix} \begin{bmatrix} E^i_\parallel(Q_E) \\ E^i_\perp(Q_E) \end{bmatrix} \; s' \; e^{jks'\sin^2\beta_o} \; e^{jk\overline{RD}\cdot\hat{D}} \qquad (3\text{-}47)$$

where $\lim\limits_{s\to\infty} \dfrac{e^{-jks}}{s}$ is suppressed and, since the phase is referenced to (x,y,z) coordinate system of the rectangular plate as shown in Figure 3-9, the phase term $e^{jk\overline{RD}\cdot\hat{D}}$ is added.
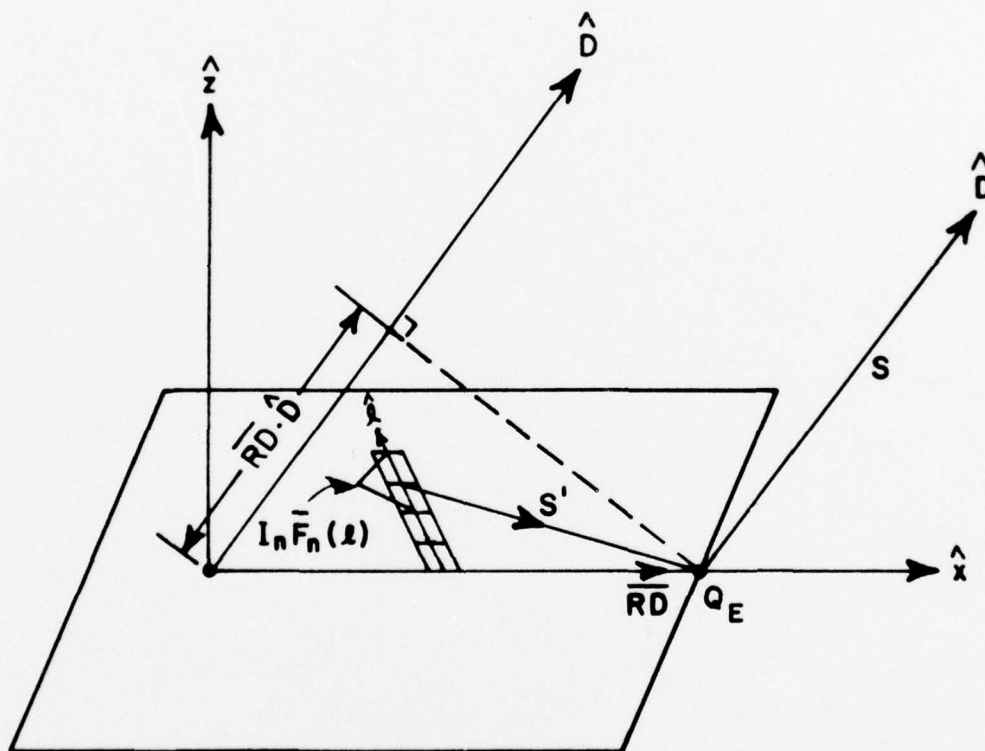
Figure 3-9. The phase reference of the far field pattern to the coordinate system of the finite ground plane.

The diffracted field just calculated may be considered as arising from a current basis function $I_n\overline{F}_n(\ell)$ defined on the nth region (Figure 3-9) of the monopoles. Therefore, the total diffracted field

is the summation of the contributions from all the current basis functions $\{I_1\bar{F}_1(\ell), I_2\bar{F}_2(\ell), \cdots I_N\bar{F}_N(\ell)\}$ including all the effects from the four edges (excluding the 2nd order diffraction and the corner diffraction).

In general, the total far field can be written as

$$\bar{E}_{total} = \sum_{n=1}^{N} \bar{E}_n^i + \bar{E}_n^r + \bar{E}_n^d \qquad (3\text{-}48)$$

where $\bar{E}_n^i$, $\bar{E}_n^r$ and $\bar{E}_n^d$ represent respectively the direct incident field, reflected field and diffracted field due to the current basis function $I_n \bar{F}_n(\ell)$ defined on the region n of the monopoles.

i. Single monopole on a rectangular plane

Consider a quarter wavelength monopole excited with 1 volt generator on a ground plane as shown in Figure 3-10. In Figure 3-11, the calculated θ-component of the far field pattern including diffraction by the 4 edges is compared with that obtained by Burnside's GTD computer program [13] for the following cases:

a) $x_1=x_2=y_1=y_2=3\lambda$, f=900 MHz (Figure 3-11a,b)

b) $x_1=x_2=y_1=y_2=14''$, f=800 MHz (Figure 3-11c,d)

c) $x_1=x_2=y_1=y_2=14''$, f=900 MHz (Figure 3-11e,f)

and d) $x_1=x_2=y_1=y_2=14''$, f=1000 MHz (Figure 3-11g,h)

where the pattern is calculated with the observation direction defined by $\phi=0°$, 180° and 0°<θ<180°. In Figure 3-11g,h, the discontinuity appearing around the region, θ=90° and 270°, is due to the second order diffraction from the edges which is not included in the calculations.

The reason for making the comparison with Burnside's pure GTD program is to provide an independent check on the validity of our computer program.

Burnside's program uses infinitesimally short current sources which have amplitudes and locations so as to simulate a quarter wavelength monopole with a sinusoidal current distribution.

21
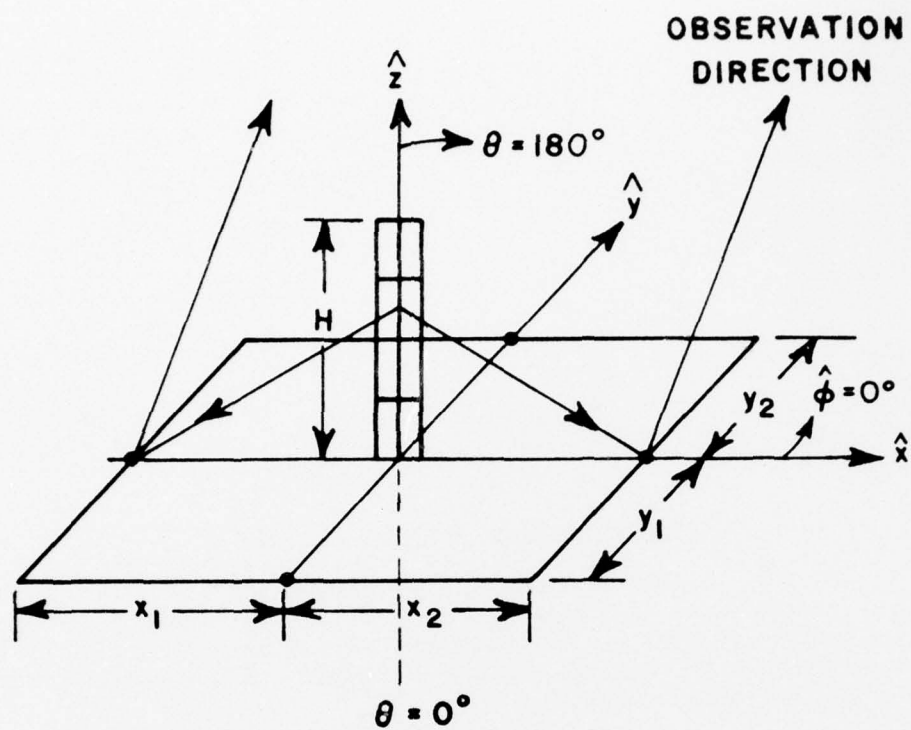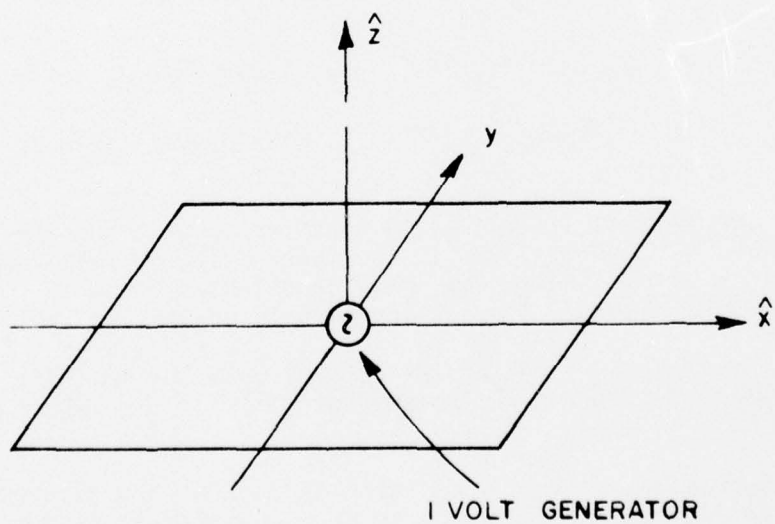
Figure 3-10. Geometry for one monopole on a finite ground plane.

22
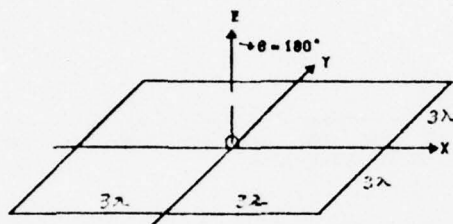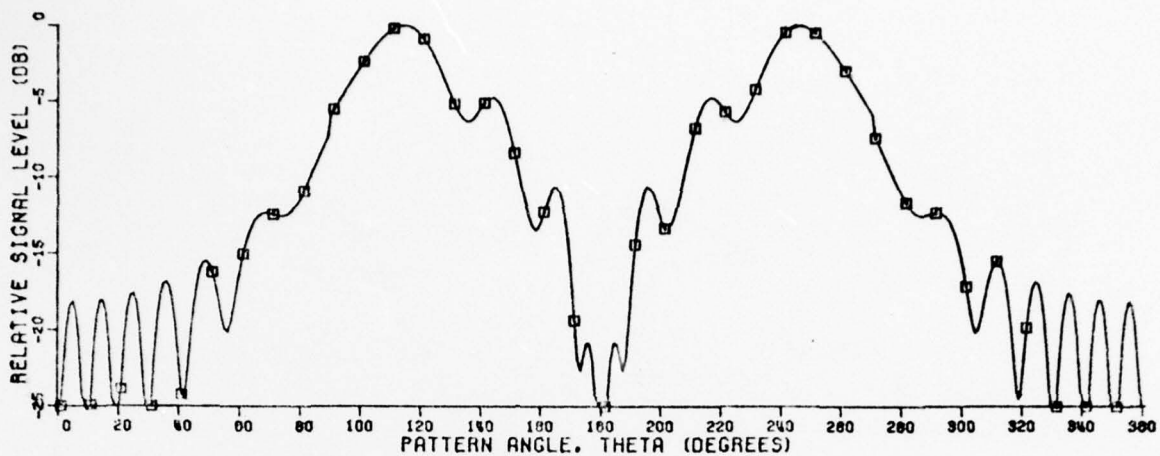
MONOPOLE TILTS AT 90.0 DEGREE

MONOPOLE LENGTH= 0.25 WAVELENGTHS

FREQUENCY= 900   MHZ

▫ PATTERN INCLUDING 4 EDGES DIFFRACTION

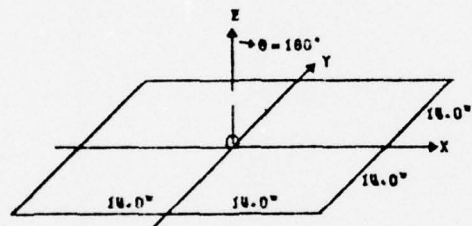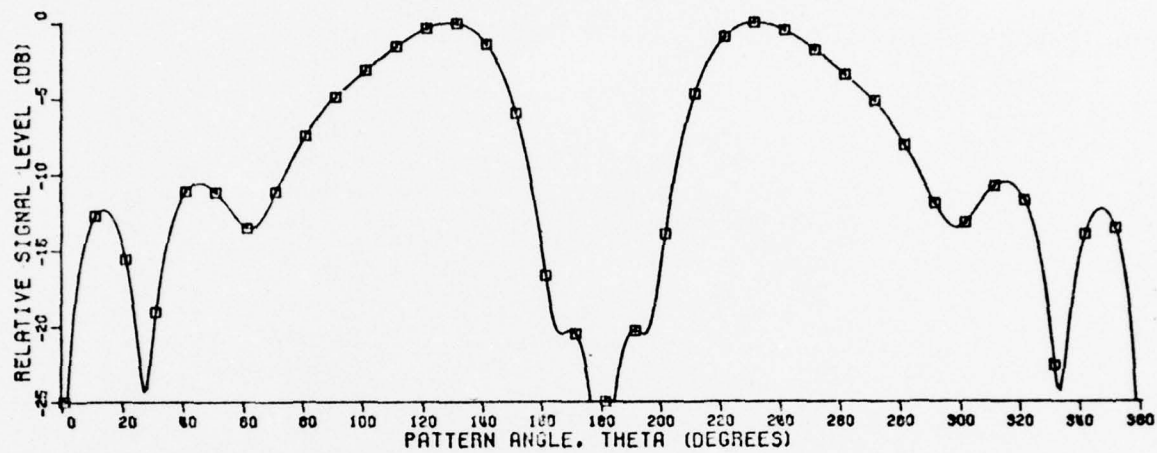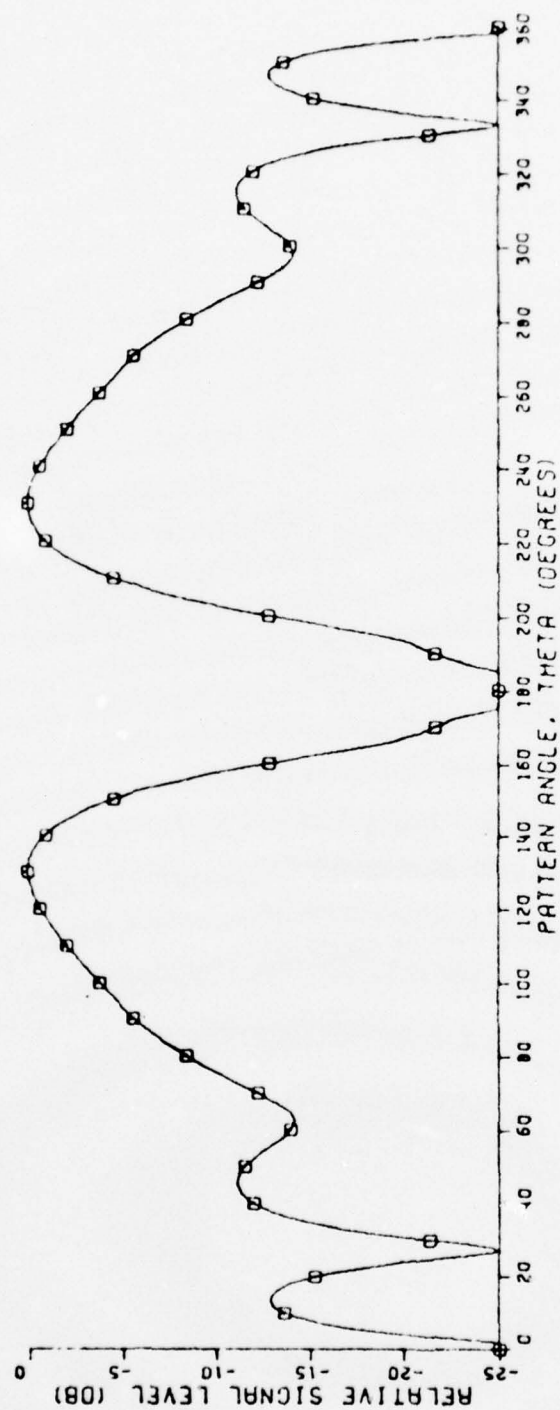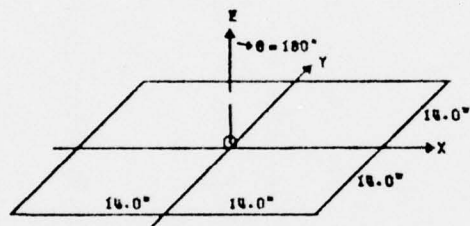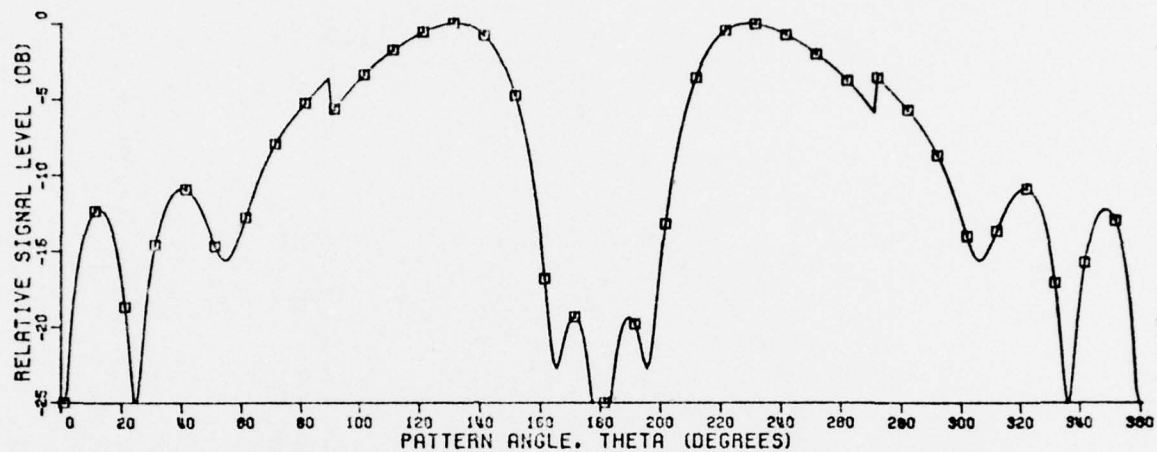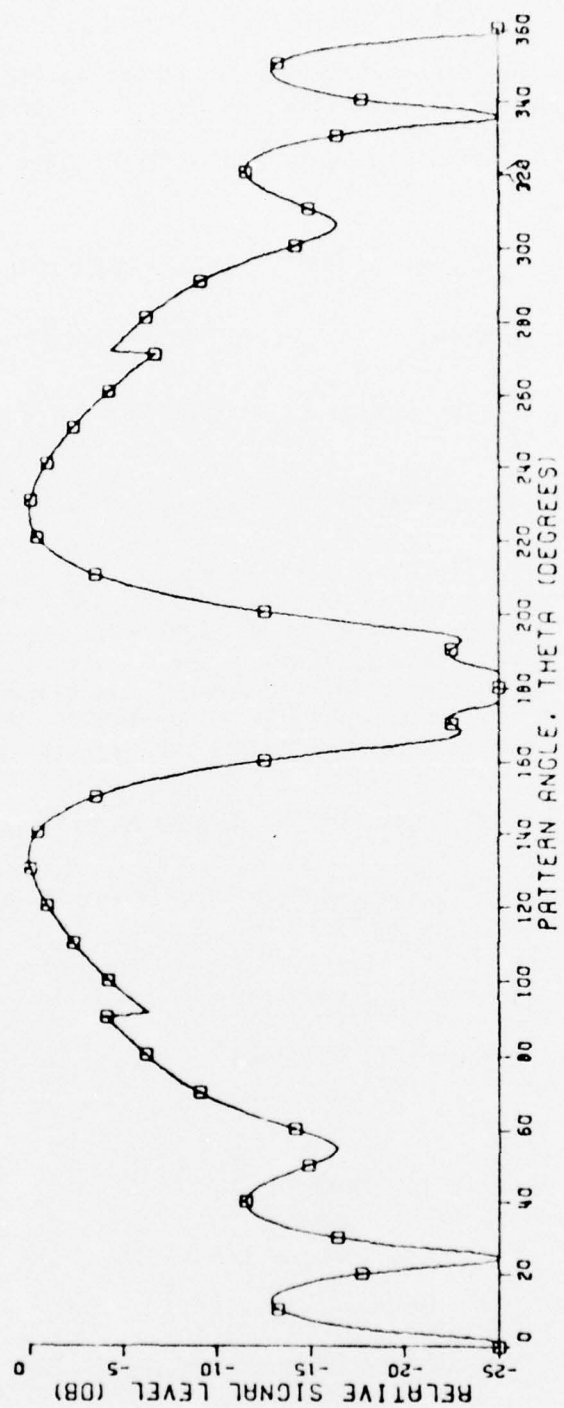Figure 3-11(a). E$_\theta$ pattern of a stub calculated by the hybrid technique.
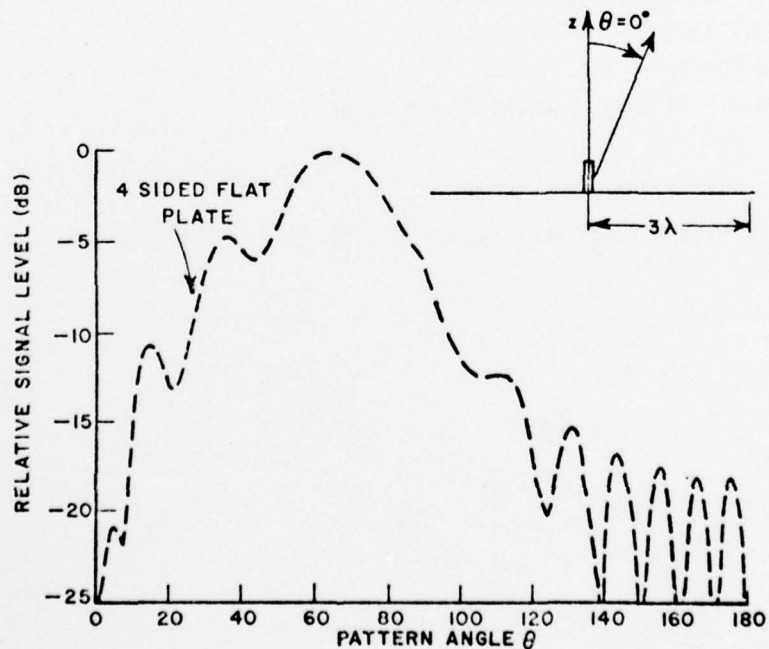
Figure 3-11(b). E$_\theta$ pattern of a stub calculated by Burnside's GTD program.

23
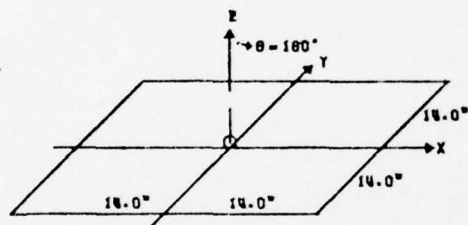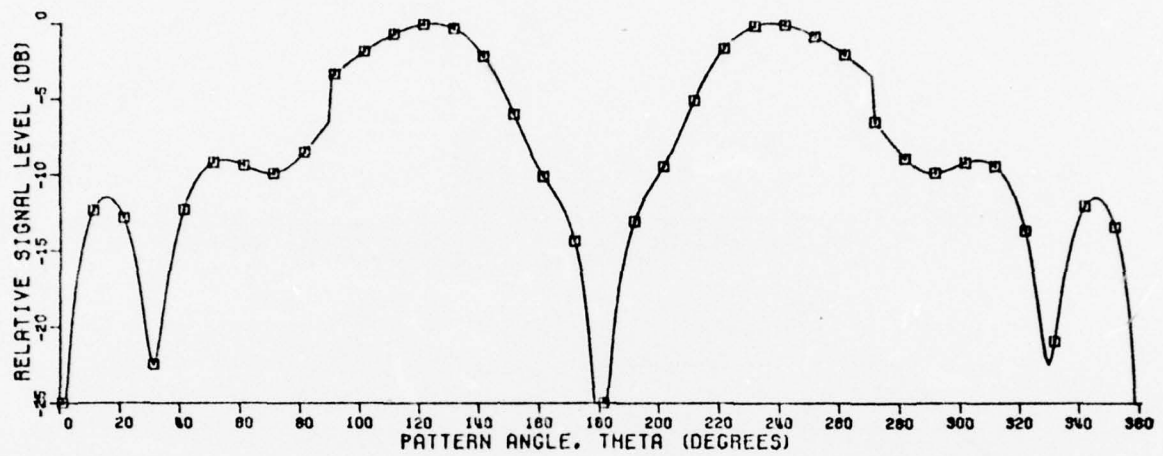
MONOPOLE TILTS AT 90.0 DEGREE
MONOPOLE LENGTH= 0.25 WAVELENGTHS
FREQUENCY= 800   MHZ
□PATTERN INCLUDING 4 EDGES DIFFRACTION

Figure 3-11(c). E_θ pattern of a stub calculated by the hybrid technique.

Figure 3-11(d). E_θ pattern of a stub calculated by Burnside's GTD program.

25

Figure 3-11(e). E_θ pattern of a stub calculated by the hybrid technique.
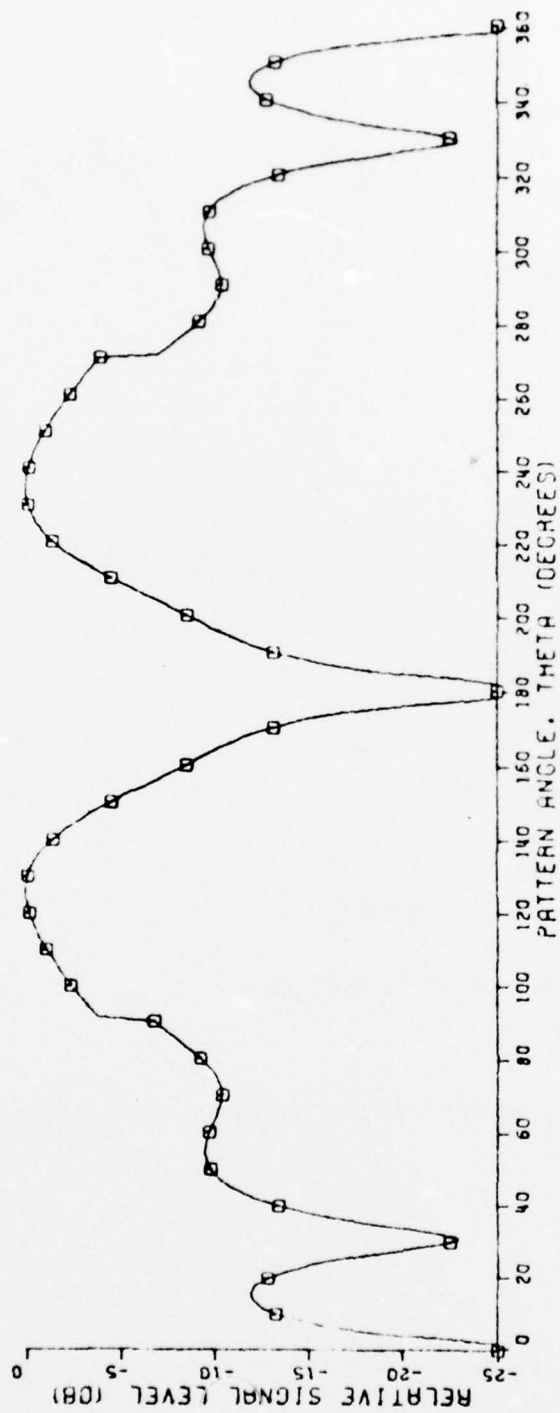
Figure 3-11(f). E_θ pattern of a stub calculated by Burnside's GTD program.

MONOPOLE TILTS AT 90.0 DEGREE
MONOPOLE LENGTH= 0.25 WAVELENGTHS
FREQUENCY= 1000 MHZ
☐ PATTERN INCLUDING 4 EDGES DIFFRACTION

Figure 3-11(g). E_θ pattern of a stub calculated by the hybrid technique.

28

Figure 3-11(h). E_θ pattern of a stub calculated by Burnside's GTD program.

ii. Two tilted monopoles on a rectangular plate

Consider two quarter wavelength monopoles tilted at an angle of $20°$ on a ground plane excited with generators as shown in Figure 3-12. The θ-component of the far field pattern including diffraction by the 4 edges is compared with that obtained by Burnside's GTD computer program for the following cases:

a) $x_1=y_1=8"$, $x_2=y_2=20"$, f=1000 MHz (Figure 3-13a,b)

b) $x_1=x_2=y_1=y_2=14"$, f=900 MHz   (Figure 3-13c,d)

c) $x_1=y_1=12"$, $x_2=y_2=16"$, f=800 MHz   (Figure 3-13e,f)

where the observation direction is given by $\phi=0°$, $180°$ and $0°\leq\theta\leq180°$.

It is noted that in both cases i and ii, the ϕ-component of the far field pattern observed in the plane $\phi=0°$, $180°$ and $0°<\theta<180°$ is zero since the antennas in these configurations have no contribution to ϕ-component in that particular observation direction. In order to see the ϕ-component of the far field pattern of two tilted antennas as mentioned in case ii, the observation plane $\phi=90°$, $270°$ and $0°\leq\theta\leq180°$ is used. The result is shown in Figure 3-14 for the cases:

a) $x_1=y_1=8"$, $x_2=y_2=20"$, f=1000 MHz (Figure 3-14a)

b) $x_1=y_1=12"$, $x_2=y_2=16"$, f=800 MHz   (Figure 3-14b)

C. Helical Antenna on a Ground Plane

The helical antenna [14] as shown in Figure 3-15a is described by the following symbols:

        D = diameter of helix
        C = circumference of helix
        S = spacing between turns
        α = pitch angle
        L = length of 1 turn
        N = number of turns
        A = axial length
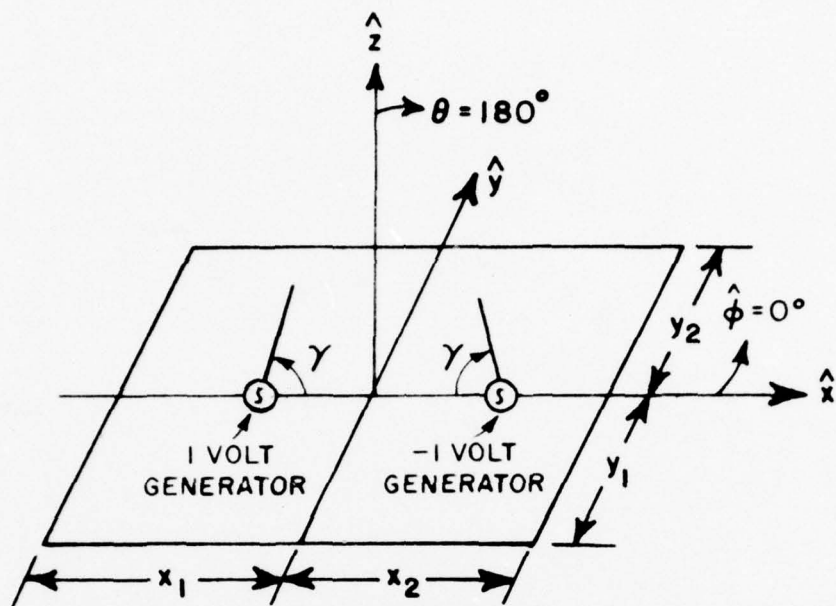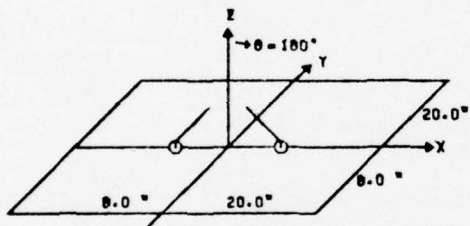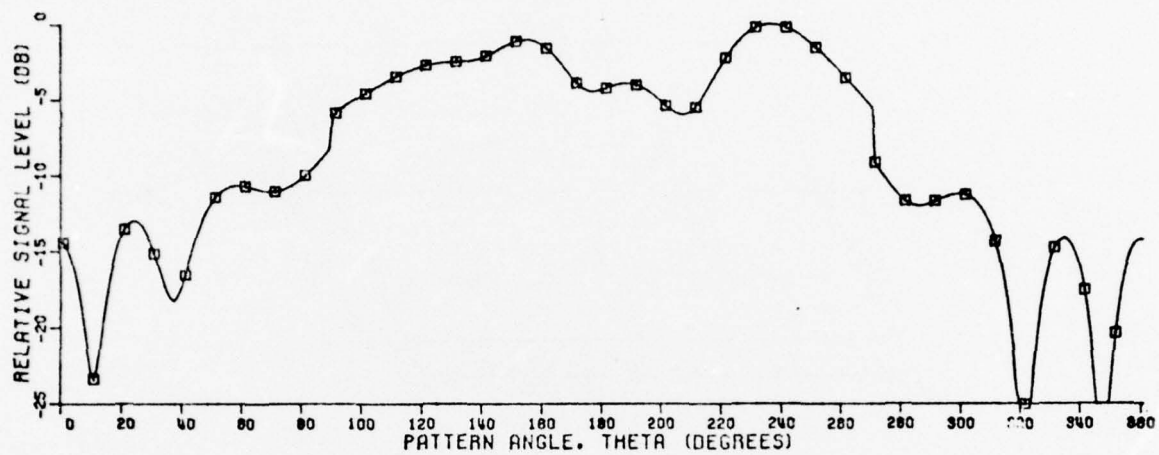   d = diameter of helix conductor.

30
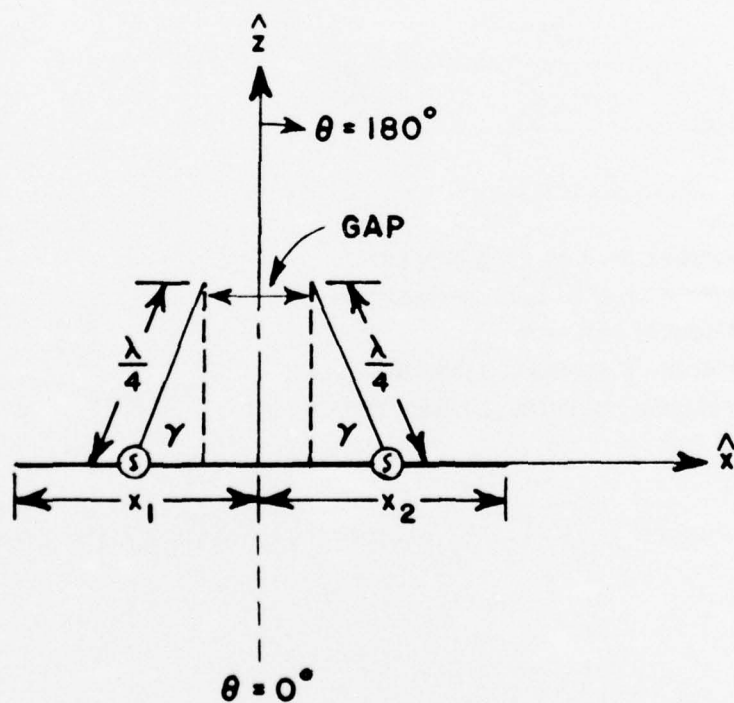
Figure 3-12. (a) 3-dimensional geometry of two tilted monopoles on a finite ground plane.

(b) 2-dimensional geometry of two tilted monopoles on a finite ground plane.

31

MONOPOLES TILT AT 20.0 DEGREE
MONOPOLE LENGTH= 0.25 WAVELENGTHS
FREQUENCY= 1000 MHZ
GAP BETWEEN ANTENNAS TIPS= 0.2 INCHES
□ PATTERN INCLUDING 4 EDGES DIFFRACTION

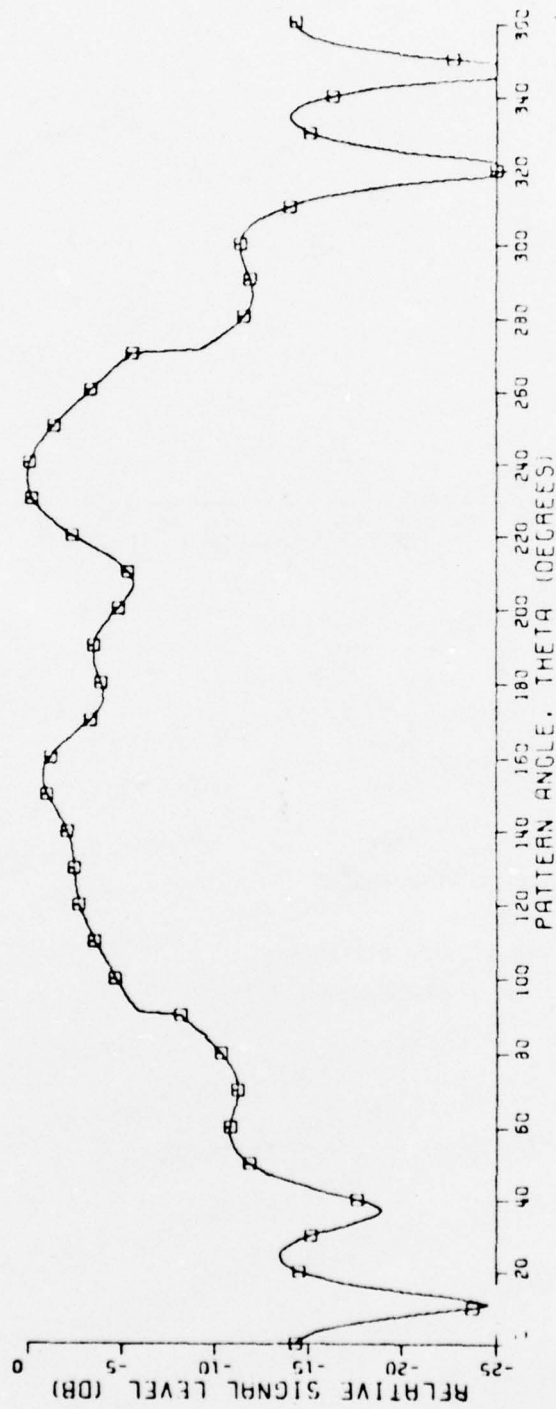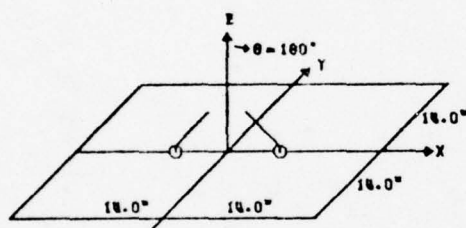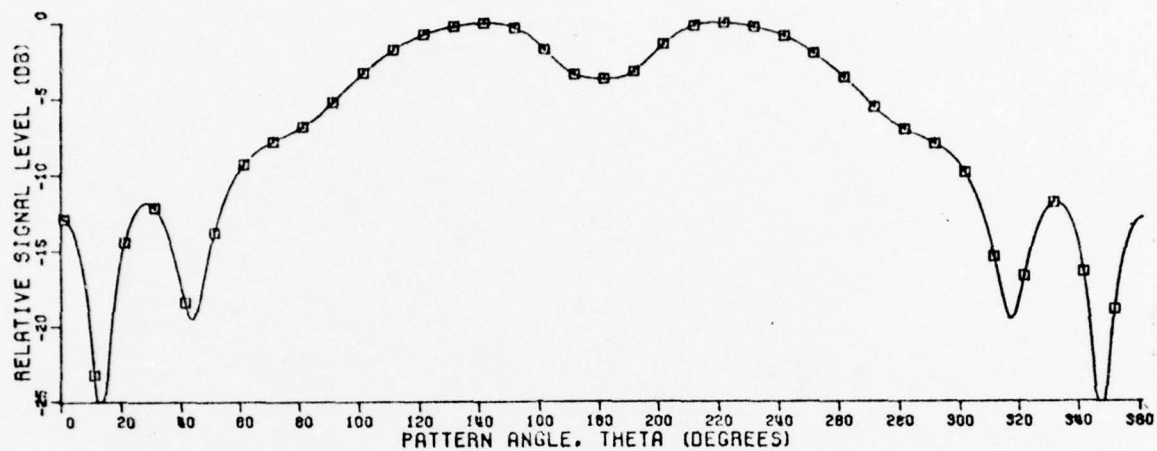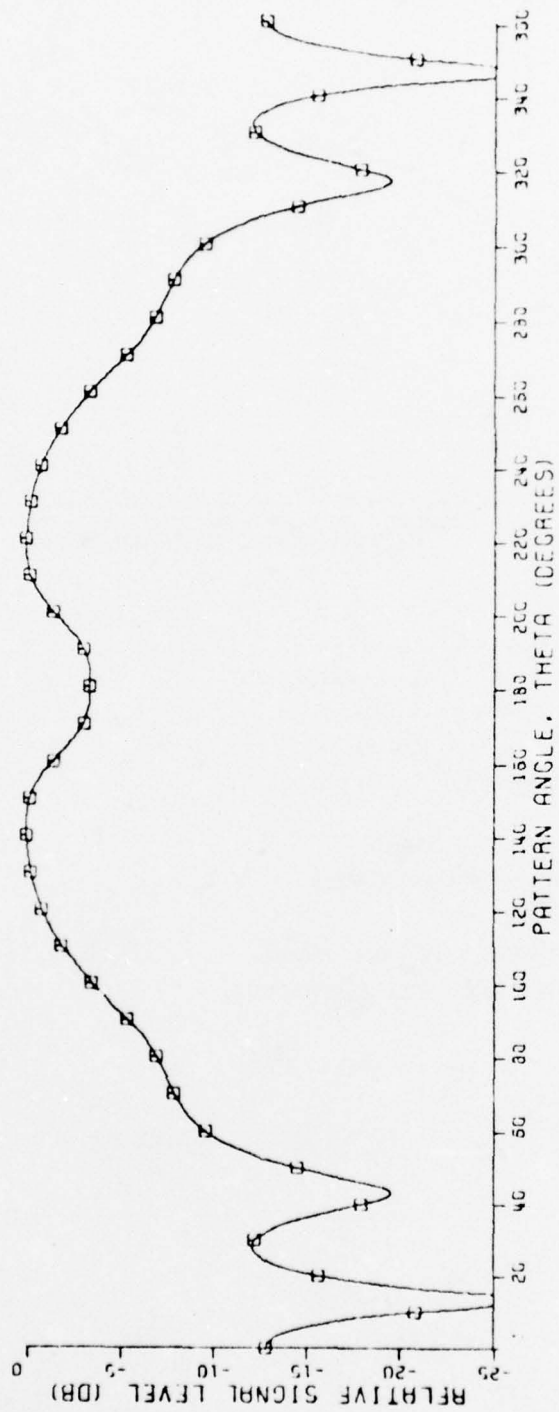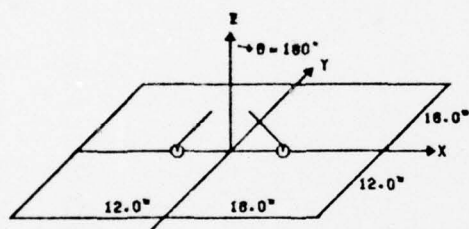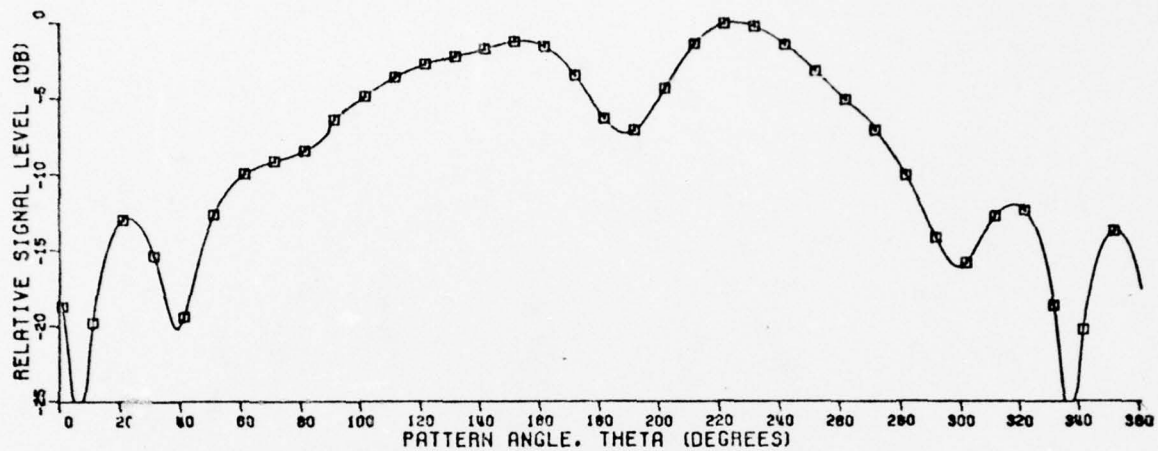Figure 3-13(a). E_θ pattern calculated by the hybrid technique.

Figure 3-13(b). E$_\theta$ pattern calculated by Burnside's GTD program.

33

MONOPOLES TILT AT 20.0 DEGREE

MONOPOLE LENGTH= 0.25 WAVELENGTHS

FREQUENCY= 900   MHZ

GAP BETWEEN ANTENNAS TIPS= 0.2 INCHES

☐ PATTERN INCLUDING 4 EDGES DIFFRACTION

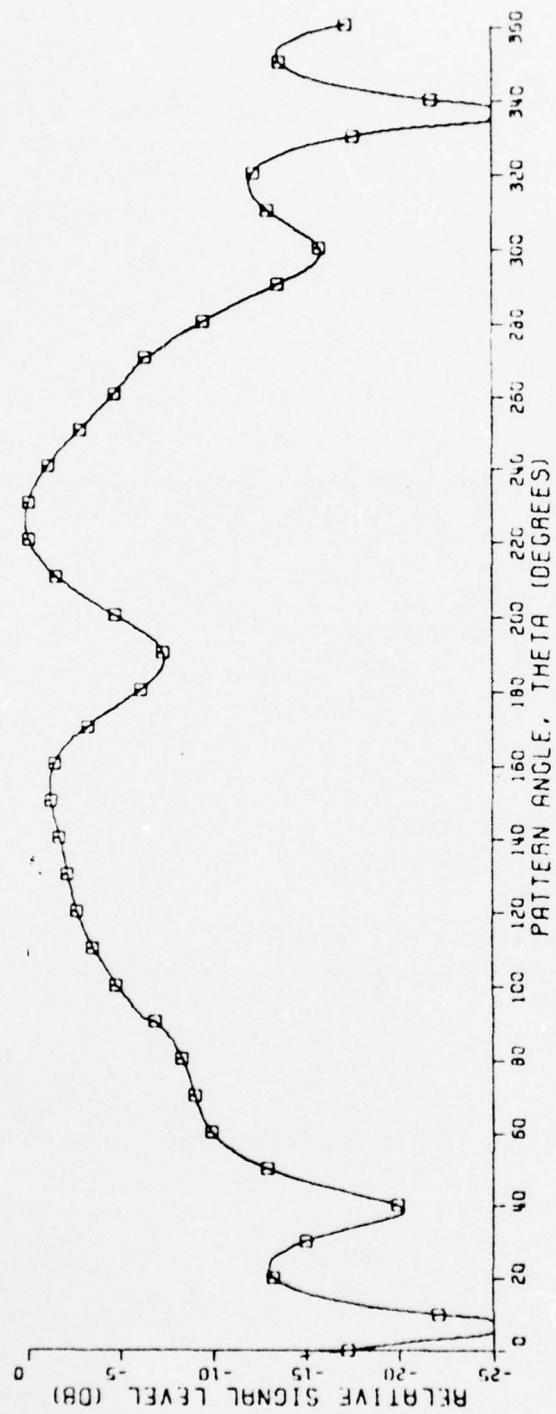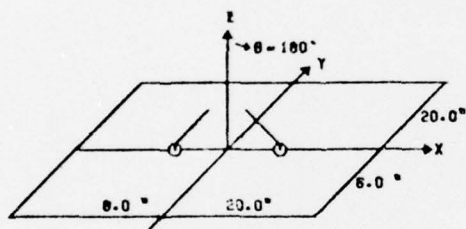Figure 3-13(c). E_θ pattern calculated by the hybrid technique.

Figure 3-13(d). E_θ pattern calculated by Burnside's GTD program.

35

RELATIVE SIGNAL LEVEL (DB)

PATTERN ANGLE. THETA (DEGREES)

MONOPOLES TILT AT 20.0 DEGREE
MONOPOLE LENGTH= 0.25 WAVELENGTHS
FREQUENCY= 800 MHZ
GAP BETWEEN ANTENNAS TIPS= 0.2 INCHES
☐ PATTERN INCLUDING 4 EDGES DIFFRACTION

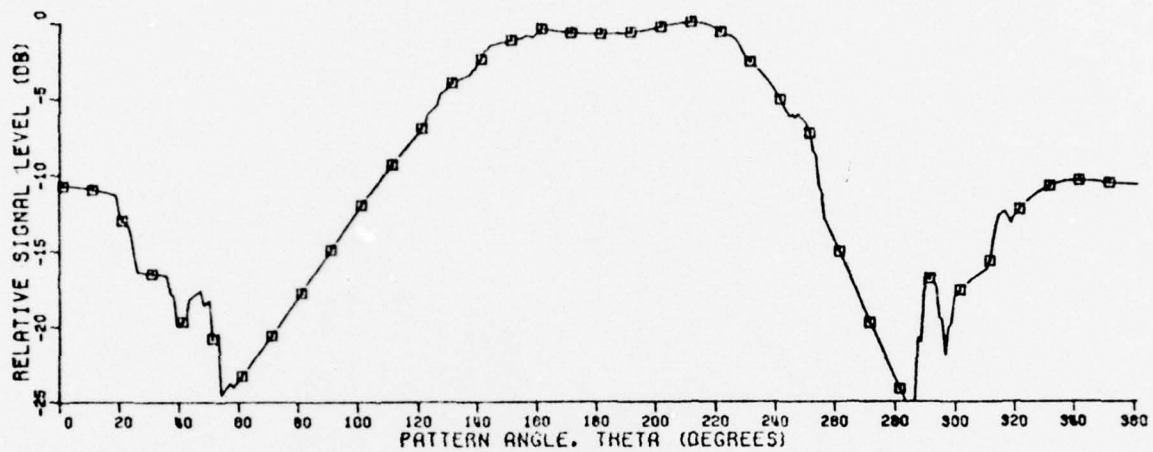Figure 3-13(e). E_θ pattern calculated by the hybrid technique.
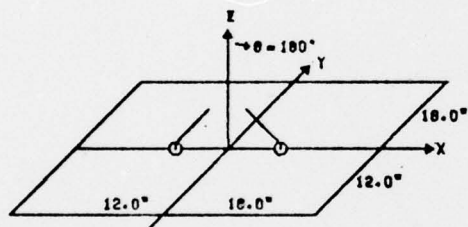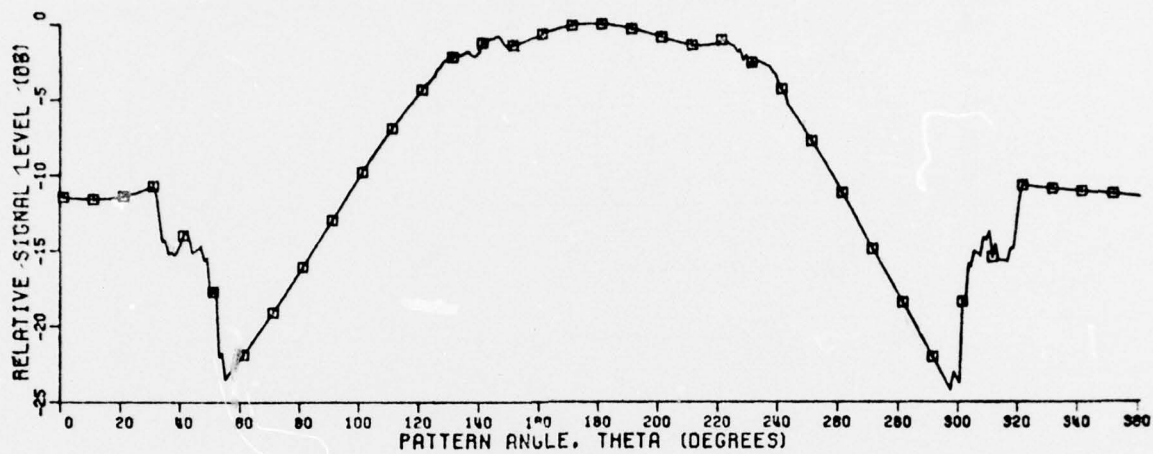
Figure 3-13(f). E_θ pattern calculated by Burnside's GTD program.

MONOPOLES TILT AT 20.0 DEGREE
MONOPOLE LENGTH= 0.25 WAVELENGTHS
FREQUENCY= 1000 MHZ
GAP BETWEEN ANTENNAS TIPS= 0.2 INCHES
▣ PATTERN INCLUDING 4 EDGES DIFFRACTION

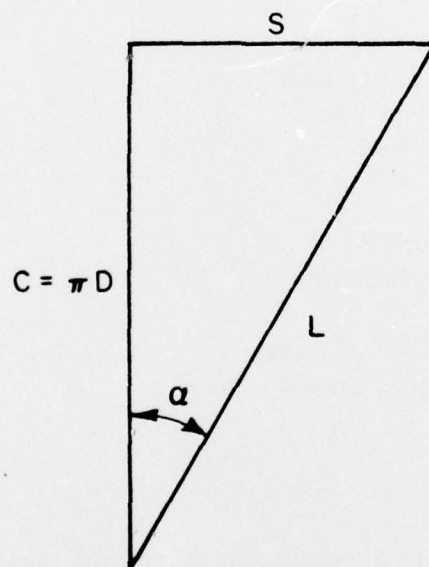Figure 3-14(a). E_ϕ pattern calculated by the hybrid technique.

MONOPOLES TILT AT 20.0 DEGREE
MONOPOLE LENGTH= 0.25 WAVELENGTHS
FREQUENCY= 800 MHZ
GAP BETWEEN ANTENNAS TIPS= 0.2 INCHES
□ PATTERN INCLUDING 4 EDGES DIFFRACTION

Figure 3-14(b). E_ϕ pattern calculated by the hybrid technique.
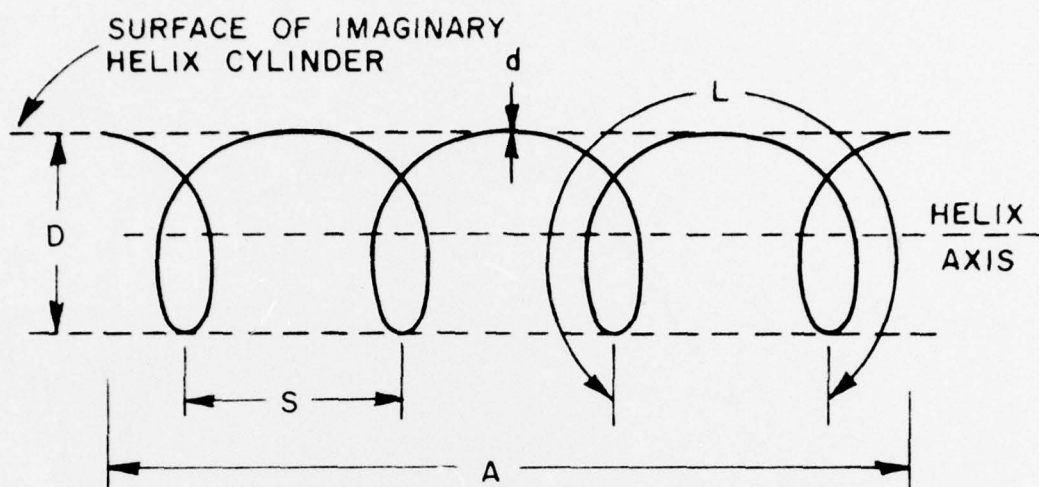
Figure 3-15. (a) Helix and associated dimension

(b) Relation between circumference, spacing, turn length, and pitch angle of one turn of a helix.

40

If 1 turn of a circular helix is stretched out straight on a flat plane, the relation between the spacing S, circumference C, turn length L and pitch angle α are as illustrated by the triangle in Figure 3-15b.

For the work presented in this report, a hexagon is used to approximate the circular helical antenna which has the terminal arrangement as shown in Figure 3-16a.

In general, although there is an infinite variety of radiating far field patterns associated with a helical antenna, two kinds are of particular interest. One is the axial or beam mode of radiation, and the other is the normal mode of radiation. For the axial mode radiation, there is a field maximum in the direction of the axis of the helical antenna and for the normal mode radiation, the field maximum occurs normal to the helix axis.

To obtain the far field pattern of a helical antenna on a finite ground plane the Hybrid technique is applied. The far field patterns of a 2-turn helix radiating in an axial mode on an infinite ground plane are shown in Figure 3-17a and b; whereas, the far field patterns of the same helix on a finite ground plane with $x_1=x_2=y_1=y_2=0.5\lambda$ are shown in Figure 3-17c and d. The pitch angle and circumference of the radiating helix are $13.965°$ and 1.0053 wavelength, respectively. The lack of complete symmetry is due to the physical connection between the helix itself and the feed point which renders the antenna geometry non-symmetrical.

For the normal mode radiation, Figure 3-18a and Figure 3-18b show the far field patterns of a one-turn helix on an infinite ground plane and a finite ground plane ($x_1=x_2=y_1=y_2=0.5\lambda$), respectively, where $\alpha=9.0341°$ and $c=0.1\pi\lambda$. The discontinuity appearing around $\theta=90°$ and $270°$ is due to the second order diffraction from the edges which is not included in the calculations. It is noted that only the E_θ-component is shown in Figure 3-18. Since the E_ϕ-component is practically zero compared with E_θ-component when observed in a plane with $\phi=90°$, $270°$ and $0°\leq\theta\leq180°$.

Furthermore, the terminal impedances of a 5-turn helix on an infinite ground plane and on a finite ground plane with $x_1=x_2=y_1=y_2=0.5\lambda$ are calculated with different frequencies and are shown in Figure 3-19a and b. The helix is approximated by hexagons with $\alpha=18°$ and $0.66\lambda\leq c\leq1.2\lambda$. The terminal impedance is highly sensitive to changes in frequency for $c<2/3\lambda$, but is nearly as constant with frequency for $3/4<c<4/3$ within which the helix is in an axial mode. The spiral form of the impedance can be in general compared to the impedance measurement obtained by Kraus [14] as shown in Figure 3-20. The disagreement between Figure 3-19 and Figure 3-20 is due to the sensitivity of the feed point modeling. For this work, a delta gap model generator is used and no attempt is made to model the tapered feed in the vicinity of the feed point itself.

41
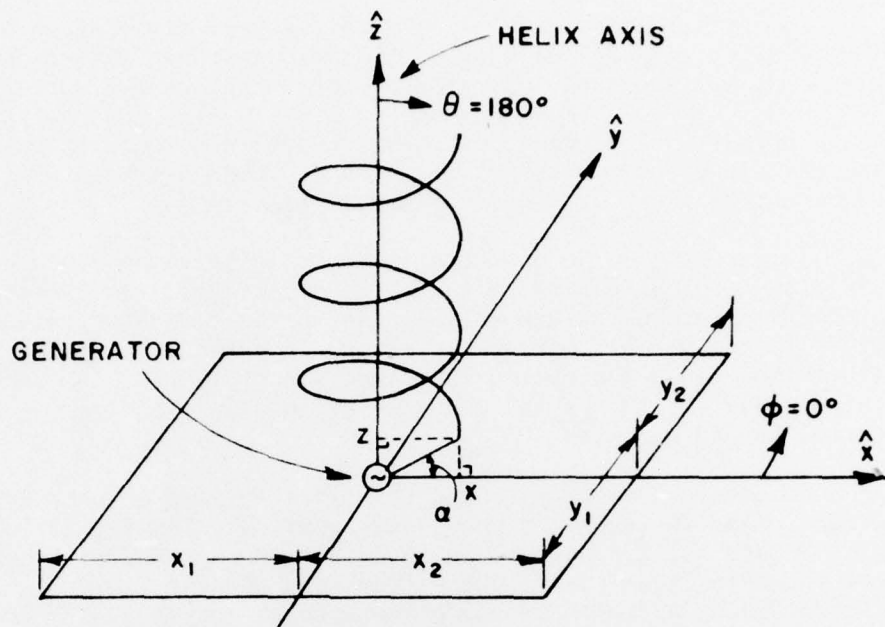
$$x = \frac{C}{2\pi} \quad , \quad y = 0 \quad , \quad z = \frac{C}{2\pi} \ \text{TAN} \ \alpha$$

(a)
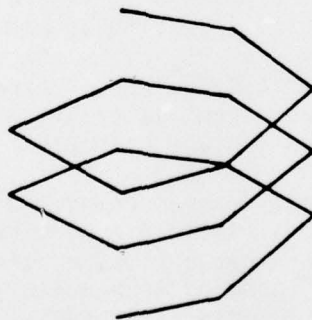
(b)

Figure 3-16. (a) Geometry for a helical antenna in a finite ground plane.
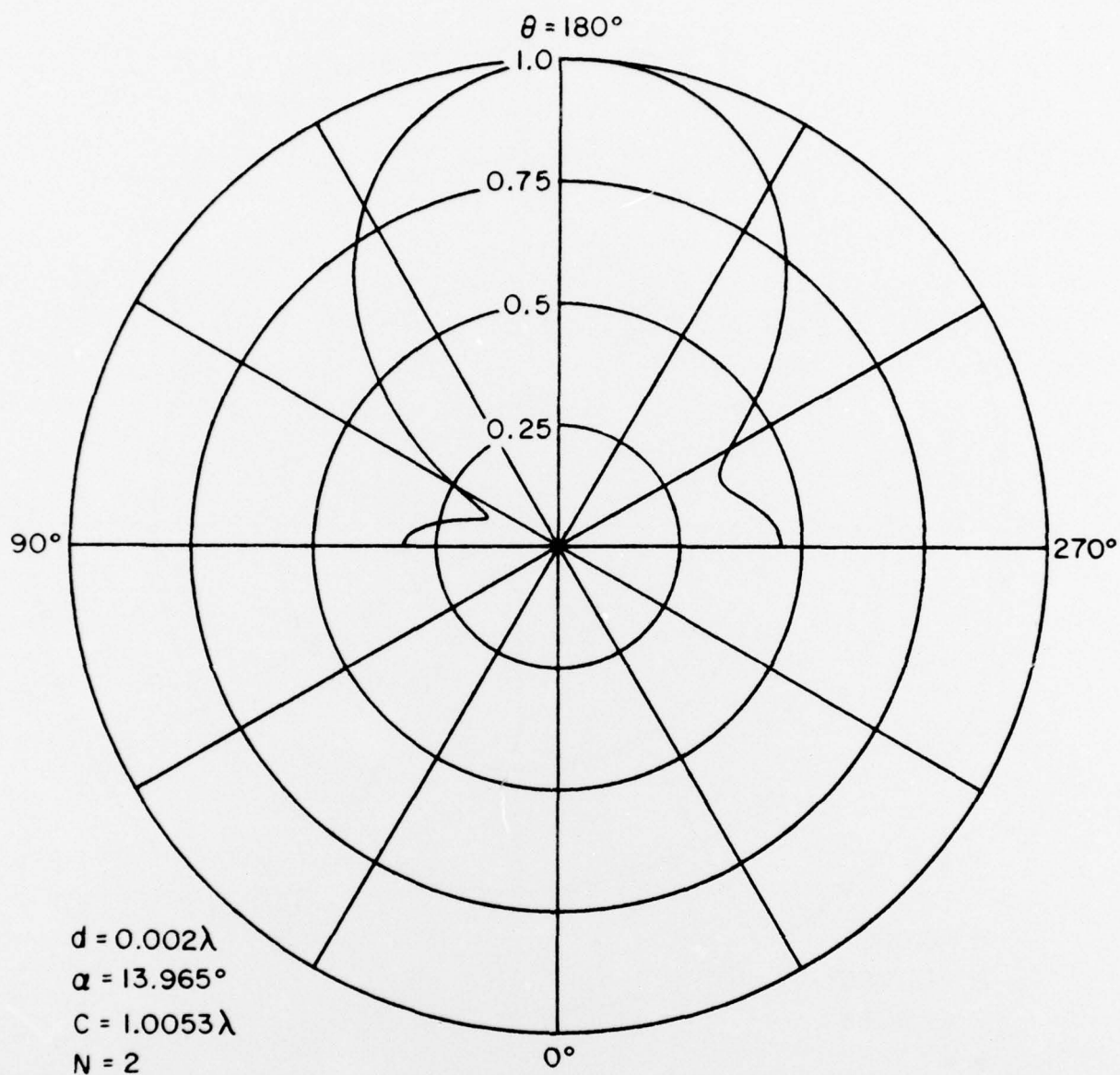
(b) Hexagons are used to approximate a circular helix.

42

θ = 180°

d = 0.002λ
α = 13.965°
C = 1.0053λ
N = 2

90°

270°

0°

Figure 3-17(a).   The calculated E_θ pattern (not in dB) of a helical
antenna on an infinite ground plane radiating in
the axial mode.   The observation plane is defined
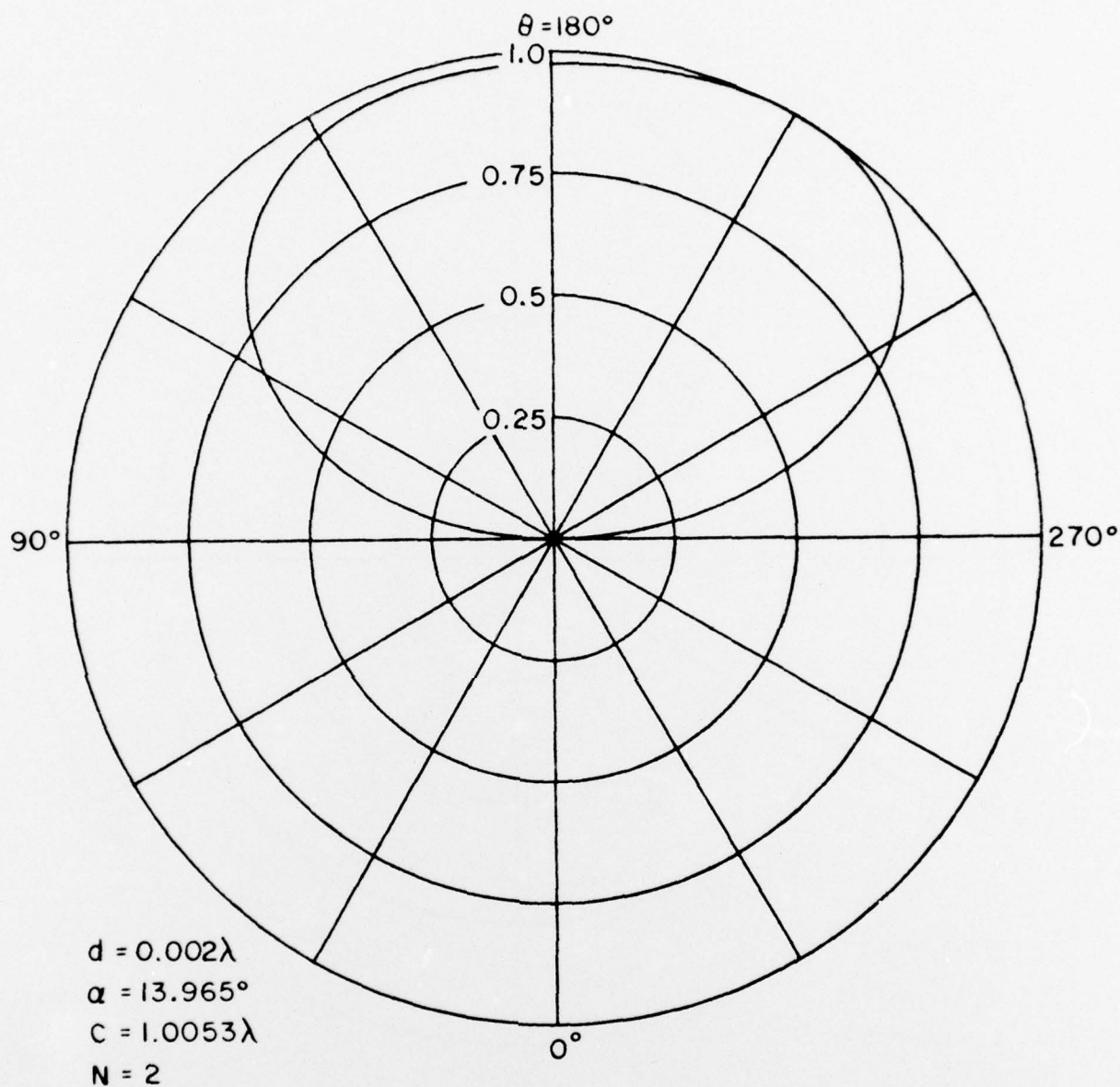by φ=90°, 270° and 0°≤θ≤180°.

43

Figure 3-17(b). The calculated E_ϕ pattern (not in dB) of a helical antenna on an infinite ground plane radiating in the axial mode. The observation plane is defined by $\phi=90°$, $270°$ and $0°\leq\theta\leq180°$.

44

Figure 3-17(c). The calculated E_θ pattern (not in dB) of a helical antenna on a finite ground plane radiating in the axial mode. The observation plane is defined as in (a).
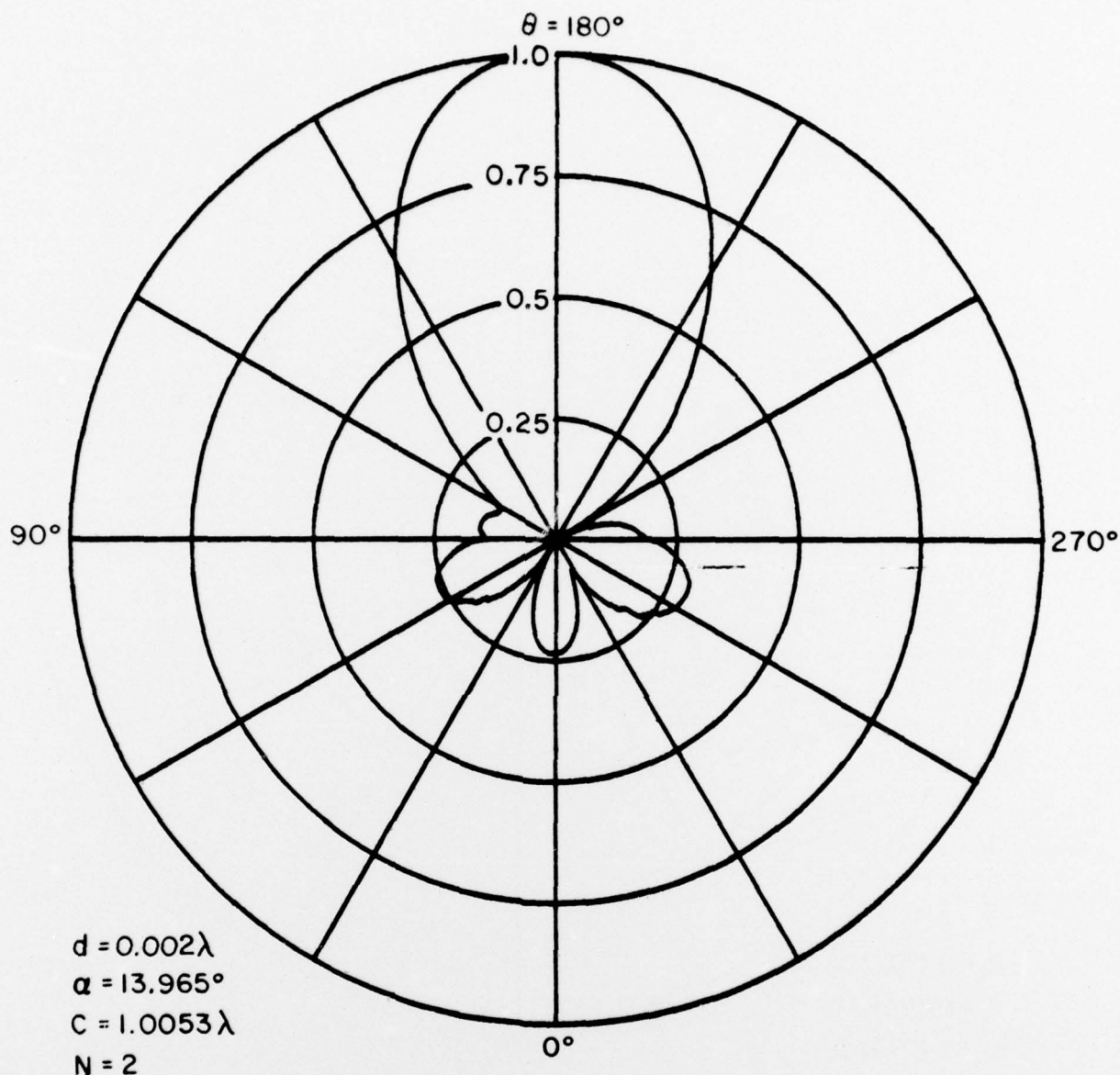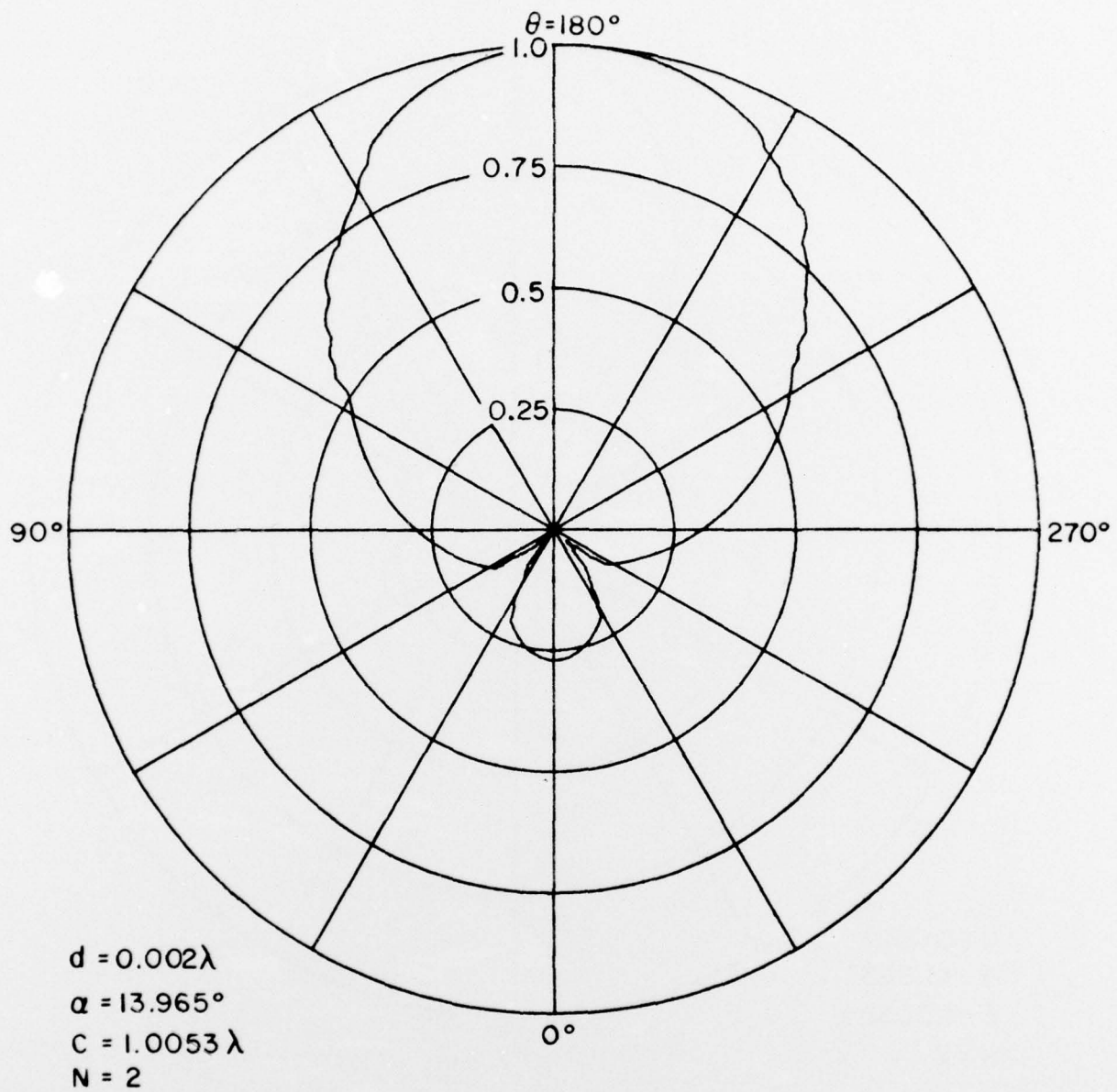
Figure 3-17(d). The calculated E_ϕ pattern (not in dB) of a helical antenna on a finite ground plane radiating in the axial mode. The observation plane is defined as in (a).
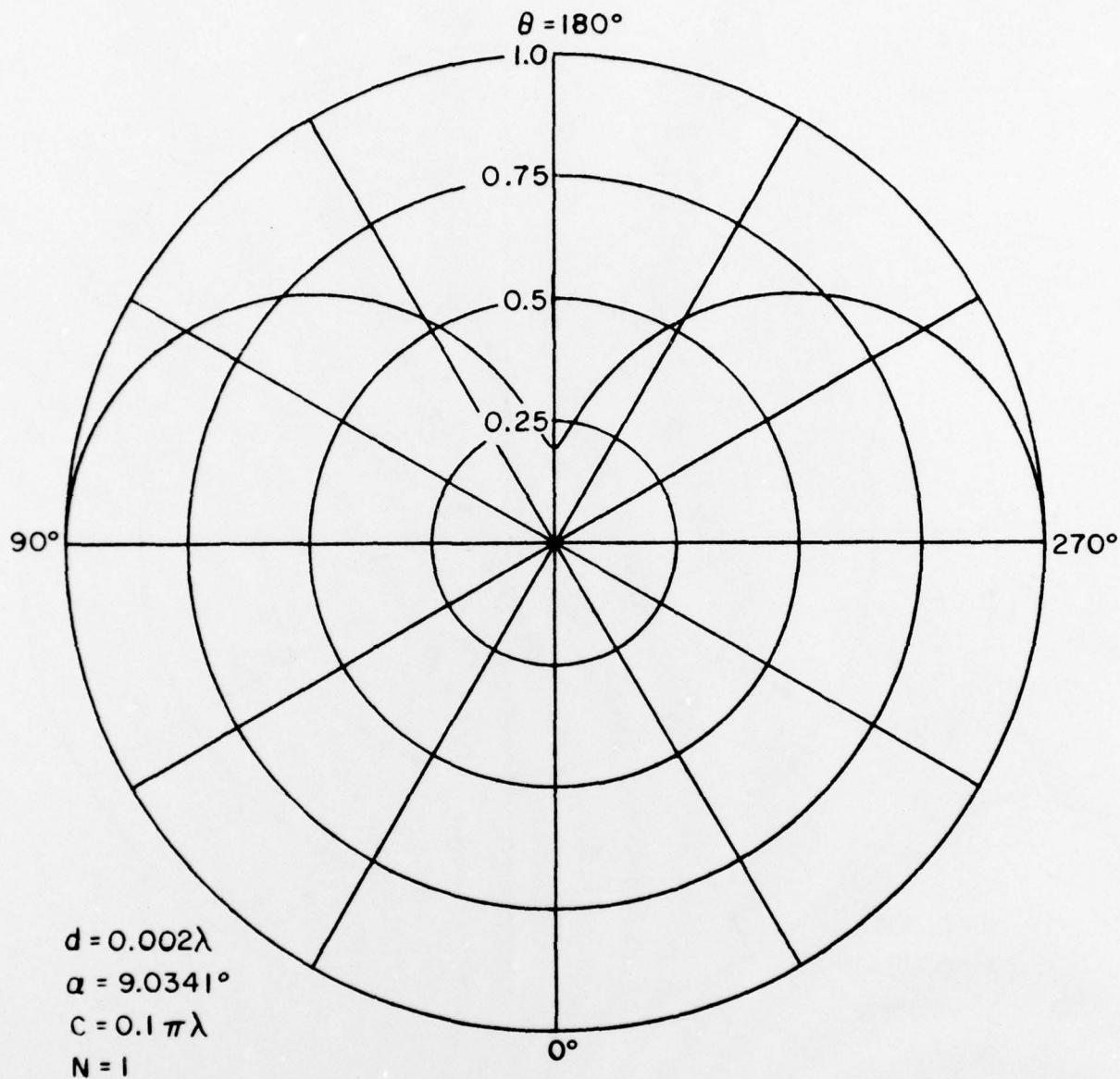
$\theta = 180°$

1.0

0.75

0.5

0.25

90°

270°

$d = 0.002\lambda$
$a = 9.0341°$
$C = 0.1\pi\lambda$
$N = 1$

0°

Figure 3-18(a). The calculated E_θ pattern (not in dB) of a helical antenna on an infinite ground plane radiating in the normal mode. The observation plane is defined by $\phi=90°$, 270° and $0°\leq\theta\leq180°$.
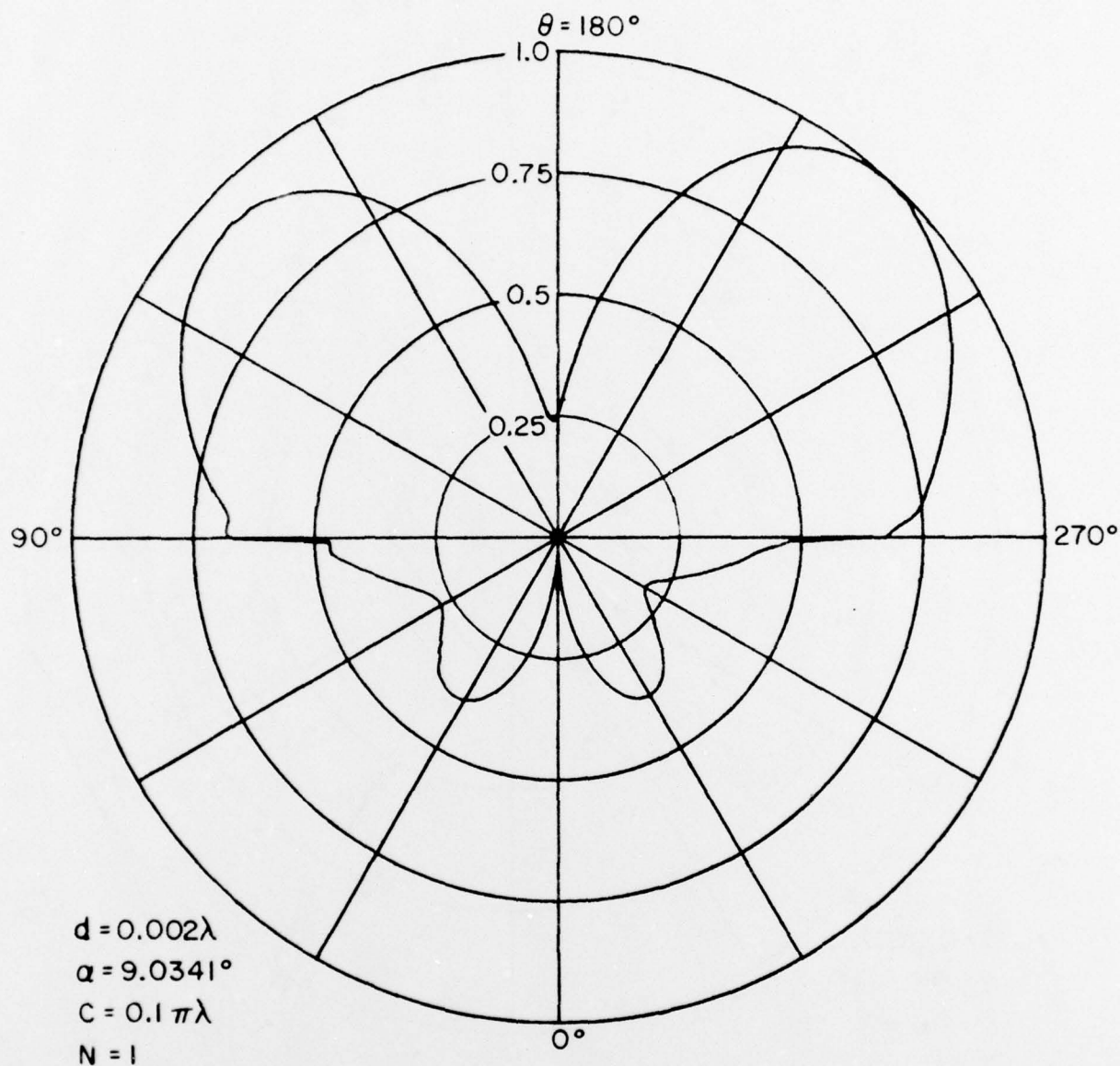
47

Figure 3-18(b). The calculated E_θ pattern (not in dB) of a helical antenna on a finite ground plane radiating in the normal mode. The observation plane is defined as in (a).
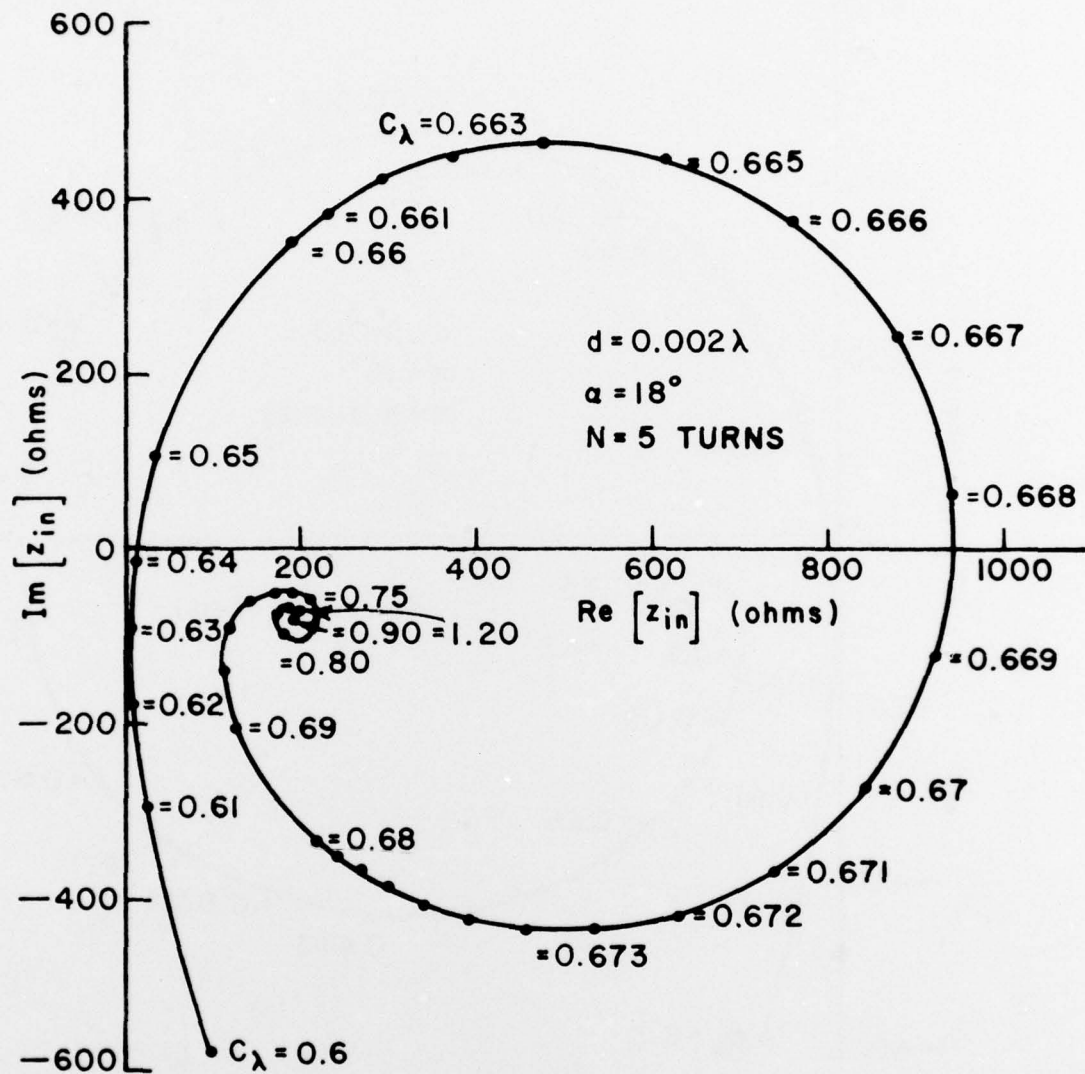
Figure 3-19(a). The calculated input impedance of a 5-turn
helix approximated by hexagons on an
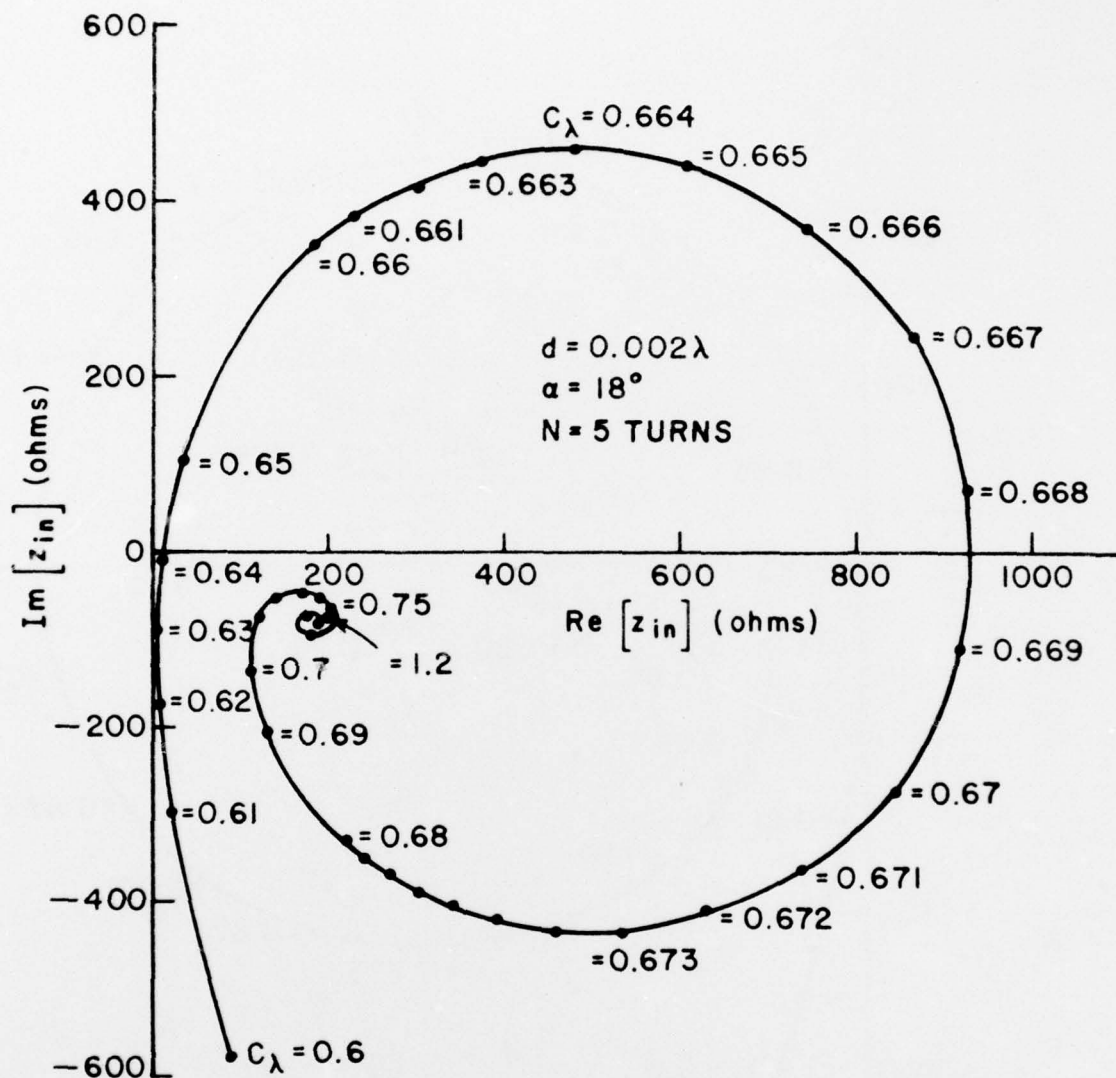infinite ground plane as a function of
frequency.

49

Figure 3-19(b). The calculated input impedance of a 5-turn helix approximated by hexagons on a finite ground plane as a function of frequency.
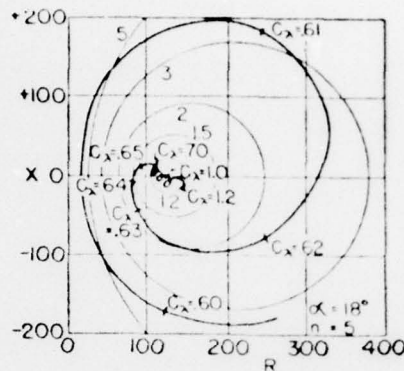
Figure 3-20. The measured input impedance of a 5-turn
helix on a ground plane as a function of
frequency is obtained by Kraus.

IV. SUMMARY AND CONCLUSION

Antennas on satellites assume many different configurations. Many
of these configurations are wire type antennas or can be modeled by
wires. In addition to modeling the antennas themselves, the satellite
body itself must also be modeled.

The work presented in this final report has shown how the modeling
of both the antennas and satellite body can best be accomplished. The
terms of interest that can be accurately calculated include impedance,
radiation patterns, coupling between antennas, response of an antenna to
another when the response antenna is loaded with a frequency sensitive
device (filter) etc.

The computer program developed in connection with the work discussed
herein is sufficiently flexible that it can be used in the design as
well as analysis of satellite antenna systems. For example, the
performance of an antenna in the presence of up to four other antennas
of arbitrary wire geometry (e.g., helix) can be calculated as a function
of frequency. The ultimate use made of such software depends in large
part upon the degree to which the program is made user orientated. One
possibility for the future is to make the program interactive through
a visual (i.e., CRT) display.

51

REFERENCES

[1] T.H. Newhouse and G.A. Thiele, "A New Method for Combining the Method of Moments with the Geometrical Theory of Diffraction," Report 3468-4, March 1974, The Ohio State University ElectroScience Laboratory, Department of Electrical Engineering; prepared under Contract N00014-67-A-0018 for Office of Naval Research (Naval Research Laboratory).

[2] C.L. Moore, Jr. and G.A. Thiele, "Satellite Antenna Pattern Distortion Due to Ground Plane Edges," Final Report 4091-2, October 1975, The Ohio State University ElectroScience Laboratory, Department of Electrical Engineering; prepared under Contract N00014-75-C-0313 for Office of Naval Research (Naval Research Laboratory).

[3] R.F. Harrington, Field Computation by Moment Methods, The Mac-millan Co., New York, 1968.

[4] G.A. Thiele, "Wire Antennas," Chapter 2 of Computer Techniques for Electromagnetics, R. Mittra, Ed., Pergamon Press, London, 1973.

[5] V.H. Rumsey, "Reaction Concept in Electromagnetic Theory," Phys. Rev., 94, June 15, 1954, pp. 1483-1491.

[6] A. Sommerfeld, Optics, Academic Press, Inc., New York, 1954, pp. 245-265.

[7] W. Pauli, "On Asymptotic Series for Functions in the Theory of Diffraction of Light," Phys. Rev., 54, 1 December 1968, pp. 924-931.

[8] R.G. Kouyoumjian, Notes for a "Short Course on Application of GTD and Numerical Techniques to the Analysis of Electromagnetics and Acoustic Radiation and Scattering," September 1973, The Ohio State University, Columbus, Ohio.

[9] J.H. Richmond, "Digital Solutions of the Rigorous Equations for Scattering Problems," Proc. of the IEEE, August 1965, pp. 796-804.

[10] J.H. Richmond, "Computer Program for Thin-Wire Structures in a Homogeneous Conducting Medium," from notes for "Short Course on Application of GTD and Numerical Techniques to the Analysis of Electromagnetic and Acoustic Radiation and Scattering," September 1973, The Ohio State University, Columbus, Ohio.

[11] W.D. Burnside, "Analysis of On-Aircraft Antenna Patterns," Report 3390-1, August 1972, The Ohio State University ElectroScience Laboratory, Department of Electrical Engineering; prepared under Contract N62269-72-C-0354 for Naval Air Development Center. (AD 777 989)

[12] R.J. Marhefka, "Analysis of Aircraft Wing-Mounted Antenna Pattern," Report 2902-25, June 1976, The Ohio State University ElectroScience Laboratory, Department of Electrical Engineering; prepared under Grant No. NGL 36-008-138 for National Aeronautics and Space Administration.

[13] W.D. Burnside, R.J. Marhefka and C.L. Yu, "Roll-Plane Analysis of On-Aircraft Antennas," IEEE Trans. on Antennas and Propagation, Vol. AP-21, No. 6, November 1973.

[14] J.D. Kraus, _Antennas_, McGraw Hill, New York, 1950.